Atomic-Scale Design of Iron Fischer-Tropsch Catalysts: A Combined Computational Chemistry, Experimental, and Microkinetic Modeling Approach

2nd Annual Report

Award Number: DE-FC26-03NT41966

Professor Manos Mavrikakis,
Professor James A. Dumesic,
Amit A. Gokhale
Rahul P. Nabar
Department of Chemical and Biological Engineering
University of Wisconsin - Madison
Madison, WI 53706

Professor Calvin H. Bartholomew,
Dr. Hu Zou,
Brian Critchfield
Department of Chemical Engineering
Brigham Young University
Provo, UT 84602

March 3, 2006

Disclaimer

Abstract

Efforts during this second year focused on four areas: (1) continued searching and summarizing of published Fischer-Tropsch synthesis (FTS) mechanistic and kinetic studies of FTS reactions on iron catalysts; (2) investigation of CO adsorption/desorption and temperature programmed hydrogenation (TPH) of carbonaceous species after FTS on unsupported iron and alumina-supported iron catalysts; (3) activity tests of alumina-supported iron catalysts in a fixed bed reactor; (4) sequential design of experiments, for the collection of rate data in a Berty CSTR reactor, and nonlinear-regression analysis to obtain kinetic parameters. Literature sources describing mechanistic and kinetic studies of Fischer-Tropsch synthesis on iron catalysts were compiled in a review. Temperature-programmed desorption/reaction methods (the latter using mass-spectrometry detection and also thermogravimetric analyzer (TGA)) were utilized to study CO adsorption/-desorption on supported and unsupported iron catalysts. Molecular and dissociative adsorptions of CO occur on iron catalysts at 25-150ºC. The amounts adsorbed and bond strengths of adsorption are influenced by supports and promoters. That CO adsorbs dissociatively on polycrystalline Fe at temperatures well below those of FT reaction indicates that CO dissociation is facile and unlikely to be the rate-limiting step during FTS. Carbonaceous species formed after FT reaction for only 5 minutes at 200ºC were initially hydrogenated under mild, isothermal condition (200ºC and 1 atm), followed by TPH to 800ºC. During the mild, isothermal hydrogenation, only about 0.1-0.2 mL of atomic carbon is apparently removed, while during TPH to 800ºC multilayer equivalents of atomic, polymeric, carbidic, and graphitic carbons are removed. Rates of CO conversion on alumina-supported iron catalysts at 220-260ºC and 20 atm are correlated well by a Langmuir-Hinshelwood expression, derived assuming carbon hydrogenation to CH and OH recombination to water to be rate-determining steps. In the coming year, studies will focus on quantitative determination of the rates of kinetically-relevant elementary steps on Fe catalysts with/without K and Pt promoters and at various levels of Al_2O_3 support, providing a database for understanding (1) effects of promoter and support on elementary kinetic parameters and (2) for validation of computational models that incorporate effects of surface structure and promoters. Kinetic parameters will be incorporated into a microkinetics model, enabling prediction of rate without invoking assumptions, e.g. of a rate-determining step or a most-abundant surface intermediate. Calculations using periodic, self-consistent Density Functional Theory (DFT) methods were performed on two model surfaces: (1) Fe(110) with ¼ ML subsurface carbon, and (2) Fe(110) with ¼ ML Pt adatoms. Reaction networks for FTS on these systems were characterized in full detail by evaluating the thermodynamics and kinetics of each elementary step. We discovered that subsurface C stabilizes all the reactive intermediates, in contrast to Pt, which destabilizes most of them. A comparative study of the reactivities of the modified-Fe surfaces against pure Fe is expected to yield a more comprehensive understanding of promotion mechanisms for FTS on Fe.

Table of Contents

Introduction

A. Background

Fischer-Tropsch Synthesis (FTS) has been used commercially for more than 70 years in the conversion of syngas (H_2/CO), derived from coal or natural gas, into liquid hydrocarbons [1,2]. Its application to production of liquid fuels from natural gas (GTL) is expanding into a large world-wide industry, while its application to conversion of syngas from renewable biomass is being researched. Gasoline and diesel fuels produced from FT synthesis are premium products of low aromaticity and zero sulfur content. Although FTS is in some respects a "mature technology", substantial improvements have been realized during the past three decades in catalyst, reactor, and process technologies as a result of intensive research. Moreover, improvements could yet be realized in catalyst and reactor design through a deeper fundamental understanding of the reaction mechanism and catalyst activity-structure relationships. Combined application of modern surface science and computational chemistry tools is a powerful methodology for realizing deeper understanding required for improving catalyst design.

Almost 80 years ago, Fischer and Tropsch postulated that CO hydrogenation takes place on bulk carbides of Co and Fe. Over the decades a consensus has emerged that FTS is a polymerization process involving addition of a CH_x (x = 0-2) monomer to a growing hydrocarbon chain. The formation of the surface CH_x is proposed to occur via adsorption of CO on a metal site and dissociation of CO to a surface carbon atom, i.e. a surface carbide (C(ad)), followed by stepwise addition of H atoms to produce methylidyne (CH(ad)), methylene (CH_2(ad)) methyl (CH_3(ad)) species. However, there is little quantitative information regarding the potential energies of these intermediates or the kinetic parameters for these and the subsequent elementary steps producing hydrocarbons. Moreover, there is little consensus regarding the mechanisms of C-C coupling, i.e. which of the CH_x species are involved in this important step for either Co or Fe catalysts.

Both Co and Fe catalysts have been used commercially for FTS. Fe catalysts were used for 55 years at Sasol for conversion of coal to fuels and chemicals because of their low cost and ability to process coal syngas having low H_2/CO ratios as a result of their high activities for the water gas shift reaction. For the same reason Fe catalysts are favored for production of fuels from biomass. Since Co catalysts are more productive and stable than Fe catalysts, they are presently favored in GTL processes; nevertheless, the low cost and low methane selectivity of Fe catalysts make them an attractive option, especially if more productive, stable, supported Fe catalysts can be developed. A microkinetics model for Fe FTS could enable the needed improvements in design. There are no previously reported microkinetic studies of FTS on Fe.

This report describes progress made during the second year of a three-year DOE-sponsored project for advanced design of supported iron Fischer-Tropsch catalysts through development of a microkinetics model for FTS based on theoretical computations and mechanistic experiments.

The BYU catalysis research team is assisting the computations team at U. Wisconsin through study and search of literature addressing FTS kinetics and mechanisms, experimental mechanistic studies of elementary reactions, and the development of rate data for alumina supported iron FTS catalysts.

B. Work Statement

1. Objectives

The principal objective of this work is to develop and validate a detailed microkinetics submodel describing the rates of the important elementary steps that occur during FTS on the surface of an iron catalyst, which incorporates the effects of K and Pt promoters, support and of surface and subsurface carbon species on the these important elementary steps.

2. Scope

This microkinetics submodel will enable prediction of catalyst activity and hydrocarbon selectivities over a range of temperatures, pressures, and H_2/CO ratio and as a function of promoter type, and of surface carbon coverage. It will address the molecular principles that govern the relative rates of chain growth versus termination on iron FT catalysts, thereby providing a basis for maximizing desirable products (e.g. olefins, diesel liquids and waxes) while minimizing formation of undesirable products such as methane, LPG, and alcohols.

3. Tasks

To accomplish the above objectives, the proposed research has been divided into the following specific tasks to be accomplished over a period of 36 months:

Task 1: Search literature and incorporate available kinetic parameters into a microkinetics model for FT surface reactions on iron; determine consistency of available data and needs for obtaining additional parameters—this will be an ongoing task. **(BYU and UW)**

Task 2: Measure kinetic parameters for key elementary steps including CO and H_2 adsorptions/desorptions, CO dissociation, C hydrogenation, olefin adsorption on unpromoted Fe catalysts and Fe catalysts promoted with K_2O and/or Pt. Catalysts will be prepared using co-precipitation and non-aqueous, evaporative deposition methods and will be characterized by H_2 and CO adsorptions, XRD, TPR, TEM, and BET methods. Studies of elementary steps will be conducted at high pressure conditions using TPD and temperature-programmed reaction spectroscopies combined with isotopic tracer studies. **(BYU)**

Task 3: Use DFT Calculations to determine reaction thermochemistry and kinetics for key elementary steps in Tasks 1 and 2, including propagation and termination steps and steps involving reactive intermediates such as hydrogenation of CH2. Investigate effects of surface/subsurface O and C, at various concentrations, on the reactivity of Fe surfaces.

Determine effects of promoter type and concentration, coverage of surface/subsurface carbon species, and surface defects on the kinetic/thermodynamic parameters for key steps. **(UW)**

Task 4: Obtain a statistical set of rate and selectivity data on $Fe/K_2O/Pt/Al_2O_3$ catalysts over a relevant range of reaction temperatures, reactant compositions, and H_2/CO ratios at commercially relevant pressures and use these data to validate the microkinetics model**.** Data will be obtained using a Berty CSTR reactor system. **(BYU and UW)**

Task 4: Build collaborative relationships with other research groups and companies and develop proposals for funding the continuation of the proposed work and its incorporation into a comprehensive catalyst particle/reactor/process model. **(BYU and UW)**

4. Deliverables

(1) A microkinetics submodel that will enable prediction of catalyst activity and hydrocarbon selectivities over a range of temperatures, pressures, H_2/CO ratio, and as a function of promoter type, and of surface carbon coverage and address the molecular principles that govern the relative rates of chain growth versus termination on Fe FT catalysts, thereby providing a basis for maximizing desirable products.

(2) First-Principles DFT calculations of binding energies, reaction barriers, and pre-exponential factor estimates for key elementary steps in the FTS mechanism.

(3) Experimental values of kinetic parameters for key elementary steps including CO and H_2 adsorptions/desorptions, CO dissociation, C hydrogenation, and olefin adsorption on unpromoted and promoted $Fe/K_2O/Pt$ under high pressure conditions using TPD and temperature-programmed reaction spectroscopies combined with isotopic tracer studies.

(4) A statistical set of rate and selectivity data on $Fe/K_2O/Pt$ catalysts over a relevant range of reaction temperatures, reactant compositions, and H_2/CO ratios that can be used to validate mechanistic models.

Executive Summary

The principal objective of this research is to develop and validate a detailed microkinetics model which describes the rates of the important elementary steps that occur on the surface of an iron catalyst during FTS. The model will incorporate effects of K and Pt promoters, support, and surface carbon species on the important elementary steps.

Efforts during this second year focused on (1) searching/summarizing published FTS mechanistic and kinetic studies of FTS reactions on Fe catalysts; (2) investigation of CO adsorption/desorption and temperature-programmed hydrogenation (TPH) of carbonaceous species after FTS on unsupported and alumina-supported Fe catalysts; (3) activity test of alumina-supported Fe catalysts on fixed bed reactor; (4) sequential design of experiments, collection of rate data in a Berty CSTR reactor, and nonlinear-regression analysis to obtain kinetic parameters..

Work during this past year produced (1) a better mechanistic understanding of CO adsorption/desorption and carbon hydrogenation, e.g., evidence that CO dissociation on polycrystalline Fe is facile and hence unlikely to be the rate limiting step, while carbon hydrogenation is a relatively slow process and likely to be rate-limiting under reaction conditions, and (2) kinetic data and kinetic parameters of FTS over supported iron catalysts on Berty CSTR reactor.

Generally, we observe that CO adsorption at 25-150ºC on iron catalysts are of two types: molecularly-adsorbed CO and dissociatively-adsorbed CO (present as C and O atoms which recombine to CO molecules at high desorption temperatures). These two types of adsorbed CO are desorbed from unsupported polycrystalline Fe catalysts (Fe, Fe/1% K, Fe/1% Pt), at about 100ºC and 400ºC, respectively. However, for alumina-supported Fe catalysts, e.g. 20% Fe/Al_2O_3, desorption temperatures are about 90º and 280ºC. Thus, desorption temperatures are lowered slightly/significantly by the support. K and Pt promoters cause desorption temperatures to shift to higher values, while the distributions of the different types are also affected. Thus, support and promoters can significantly alter the strength and mechanism of CO adsorption on Fe. That CO adsorbs dissociatively on polycrystalline Fe at temperatures well below those of FT reaction indicates that CO dissociation is facile and unlikely to be the rate-limiting step during FTS.

Carbonaceous species formed after FT reaction for only 5 minutes at 200ºC were initially hydrogenated under mild, isothermal condition (200ºC and 1 atm), followed by TPH to 800ºC. During the mild, isothermal hydrogenation, only about 0.1-0.2 ML of atomic carbon is removed, while during TPH to 800ºC multilayer equivalents of atomic, polymeric, carbidic, and graphitic carbons are removed. The total amount of carbon deposited on the catalyst during reaction decreases substantially in the order Fe, FePt, FeK; thus, promoters facilitate gasification of carbon during reaction. Moreover, K substantially increases the fraction of active carbon deposited on the iron surface. On unpromoted Fe, a large fraction of the carbonaceous deposits are inactive forms such as iron carbide and graphitic carbons which are gasified in hydrogen at

only very high temperatures (i.e. 600-800ºC). In the case of alumina-supported Fe catalysts, a sample prepared by aqueous impregnation has the largest fraction of reactive carbons.

Supported iron catalysts prepared in this study are highly dispersed materials which attain modest CO conversion and reasonably-high C_{2+} selectivity at 250ºC and 310 psi. Accordingly, their performance in FTS is typical of some precipitated iron catalysts.

A set of designed experiments was undertaken to collect rate data in a Berty CSTR reactor at 220-260ºC and 20 atm. Rate data were fitted to various rate expressions using nonlinear-regression analysis to obtain kinetic parameters. Rates of CO conversion on alumina-supported iron catalysts are correlated well by a Langmuir-Hinshelwood expression derived assuming two steps, carbon hydrogenation to CH and OH recombination to water to be rate-determining.

In the coming year, studies will focus on quantitative determination of the rates of kinetically-relevant elementary steps on Fe catalysts with/without K and Pt promoters and at various levels of Al_2O_3 support, providing a database for understanding (1) effects of promoter and support on elementary kinetic parameters and (2) for validation of computational models that incorporate effects of surface structure and promoters. Kinetic parameters will be incorporated into a microkinetics model, enabling prediction of rate without invoking assumptions, e.g. of a rate-determining step or a most-abundant surface intermediate.

On the theoretical side, our work in the past year focused on studying various elementary steps involved in FTS on two important modifications to the Fe(110) surface (1) Fe(110) with subsurface carbon and (2) Fe(110) with Pt adatoms. Our calculations indicated that putting C into the subsurface was fairly easy, particularly as a consequence of CO dissociation on Fe. This processes causes the quasi-spontaneous formation of Fe-carbides, which then motivated us to investigate the stabilization of other intermediates on the subsurface-C modified Fe(110) surface. Thermodynamic calculations revealed that this stabilization was a strong trend for all the reactive intermediates we considered. Subsequently we determined the activation energies and frequency factors associated with each of the elementary steps which will ultimately be a key input to the final microkinetic model. Thermochemical calculations for the relative stability of Pt promoters on/in the Fe surface suggested that the most stable configuration has the Pt atom adsorbed on the Fe surface. Thus, we performed a detailed thermodynamic and kinetic analysis for the same set of elementary steps studied previously on Fe and Fe-subC model surfaces on that model surface (Fe^{Pt}). In marked contrast to the Fe-subC, most species showed a distinct destabilization on the Fe^{Pt} surface. Furthermore, an analysis of the early steps of FTS on Fe^{Pt} shows that the Pt adatom is responsible for making the Fe(110) Potential Energy Surface (PES) approach that of the corresponding PES on Co(0001) — we suggest that this is an important observation, which could explain the Pt promotion of Fe-FTS catalysis. Overall the reaction networks for both the model-systems are quite complex; a detailed microkinetic model is expected to shed more light into the fundamental mechanisms of FTS on Fe-based catalysts, for a wide range of experimental conditions.

Results and Discussion based on Experiments

A. Chemical and Physical Properties of Unsupported and Supported Fe Catalysts Prepared by Aqueous and Nonaqueous Methods

Chemical compositions, pretreatment conditions, BET surface areas and average pore diameters of unsupported and alumina-supported catalysts, prepared by aqueous and nonaqueous impregnation methods, are summarized in Table 1.

Table 1. Catalyst codes, compositions, and physical properties

Catalyst codes	Compositions	Treatment/ Temperature (ºC)	Time (h)	S_{BET} (m^2/g)	Ave. Pore Diameter (nm)
99FeA	99 wt% Fe-1 wt% Al_2O_3	drying / 110	12		
		calcination / 300	6	59	
		reduction/500	12	12	
99FeAK	98 wt% Fe-1 wt% Al_2O_3-1 wt% K	drying / 110	12		
		calcination / 300	6	56	
		reduction/500	12	14	
99FeAPt	98 wt% Fe-1 wt% Al_2O_3-1 wt% Pt	drying / 110	12		
		calcination / 300	6	51	
		reduction/500	12	10	
10FeA-W	10 wt% Fe-90 wt% Al_2O_3	drying / 110	12		
		calcination / 300	6	182	8.0
		reduction/500	12	164	7.9
10FeA-A/E	10 wt% Fe-90 wt% Al_2O_3	drying / 110	12		
		calcination / 300	6	166	9.1
		reduction/500	12	138	9.5
20FeA-A/E	20 wt% Fe-80 wt% Al-La	drying / 60~110	24		
		calcination / 300	6	156	7.7
		reduction/500	12	112	8.1

BET surface areas of calcined and reduced samples of 99FeA are 59 m^2/g and 164 m^2/g respectively. Addition of K or Pt promoter doesn't affect the surface area of unsupported samples materially. Given very similar surface areas, the unsupported Fe samples are useful polycrystalline materials for study of effects of promoter on CO adsorption/desorption properties. BET surface areas of calcined and reduced samples of 10FeA-W prepared by aqueous impregnation are 182 m^2/g and 164 m^2/g respectively (see Table 1). Both values are larger than surface areas of 10FeA-A/E and 20FeA-A/E samples prepared by evaporative deposition in

acetone/ethanol. This observation is logical given that the alumina supports for 10FeA-A/E and 20FeA-A/E samples were pre-calcined before their use in preparation of the iron catalysts; moreover the 20FeA-A/E sample is supported on a La-stabilized Al_2O_3, precalcined at high temperature. The surface areas and average pore diameters of 10FeA-A/E and 20FeA-A/E samples are nevertheless suitable for FTS. Since these supports were prestabilized, it is unlikely that the significant decreases in BET surface area during reduction are due to breakdown of the support; rather they are likely due to blockage of smaller pores by large metal crystallites formed during reduction.

B. Fe Crystallite Diameters from EDX, Compared with XRD, TEM, and H_2 Chemisorption

Energy Dispersion X-ray (EDX) analysis of alumina-supported iron catalysts reduced at 500ºC was conducted using a Tecnai F20 Analytical STEM. The resolution of the equipment for particle size identification was effectively about 5-10 nm.

Figures 1-3 are TEM images and their associated elemental energy dispersion profiles of oxygen, iron, and aluminum for 10FeA-W, 10FeA-A/E, and 20FeA-A/E catalysts, respectively. The bright areas in TEM images are attributed to iron crystallites, grey areas to catalyst support, and dark areas to the background (grid and/or holes). In the TEM image for 10FeA-W (Fig. 1, left) elemental energy dispersion analysis was conducted along a line intersecting three prominant bright spots; the element energy dispersions of Al, O, and Fe along the line are plotted in Fig. 1 (right). The observation of three intense peaks in the Fe dispersion curve, distinct of those for Al and O curves, indicates that the bright spots are due to Fe crystallites of about 20 nm in diameter; that their curves track each other closely indicates that Al and O are associated with each other, i.e., in Al_2O_3). However, the elemental energy dispersion curves of Fe for the 10FeA-A/E catalyst (Fig. 2, right) is essentially flat and of low intensity; this is likely due to a predominance in these samples of small iron crystallites having dimensions of the same order or smaller than the instrumental resolution. The Fe dispersion curve for 20FeA-A/E, containing 3-4 small, overlapping peaks of low intensity (Fig. 3, right) suggests that some fraction of the Fe crystallites may be about 5-10 nm in diameter, while others might be smaller. The EDX results for these catalysts suggesting 20 nm diameter particles in the 10FeA-W catalyst (prepared by aqueous impregna-tion) and 5-10 nm or smaller diameter crystallites in the two catalyst (10FeA-A/E, and 20FeA-A/E) prepared by nonaqueous impregnation is very consistent with estimates of particle diameter from H_2 chemisorption, TEM, and XRD measurements (see Table 2).

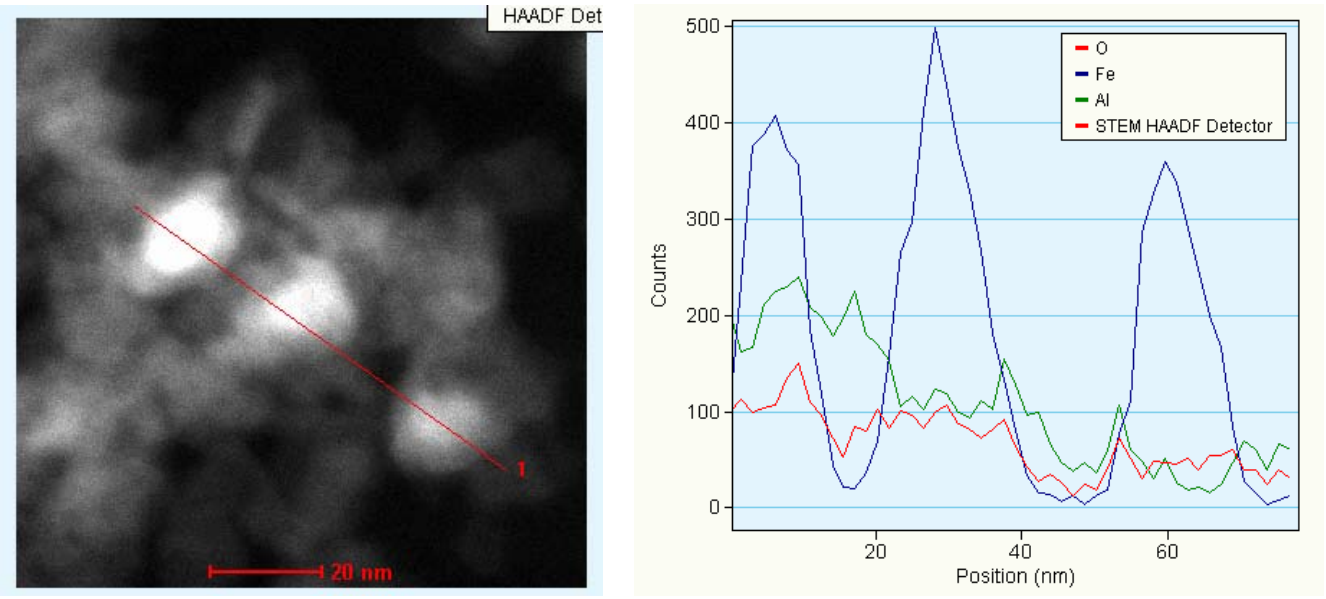

Figure 1. TEM image (left) and its associated energy dispersion (right) of elemental oxygen, iron and alumina for 10FeA-W sample.

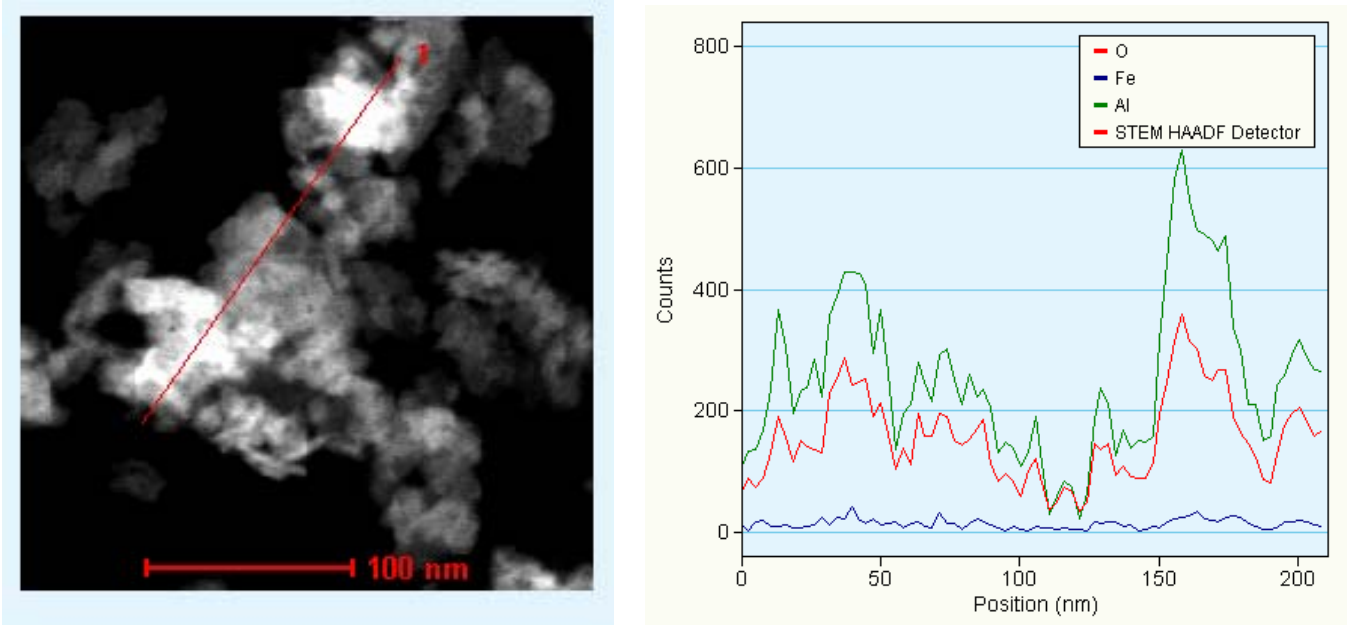

Figure 2. TEM image (left) and its associated energy dispersion (right) of elemental oxygen, iron and alumina for 10FeA-A/E sample.

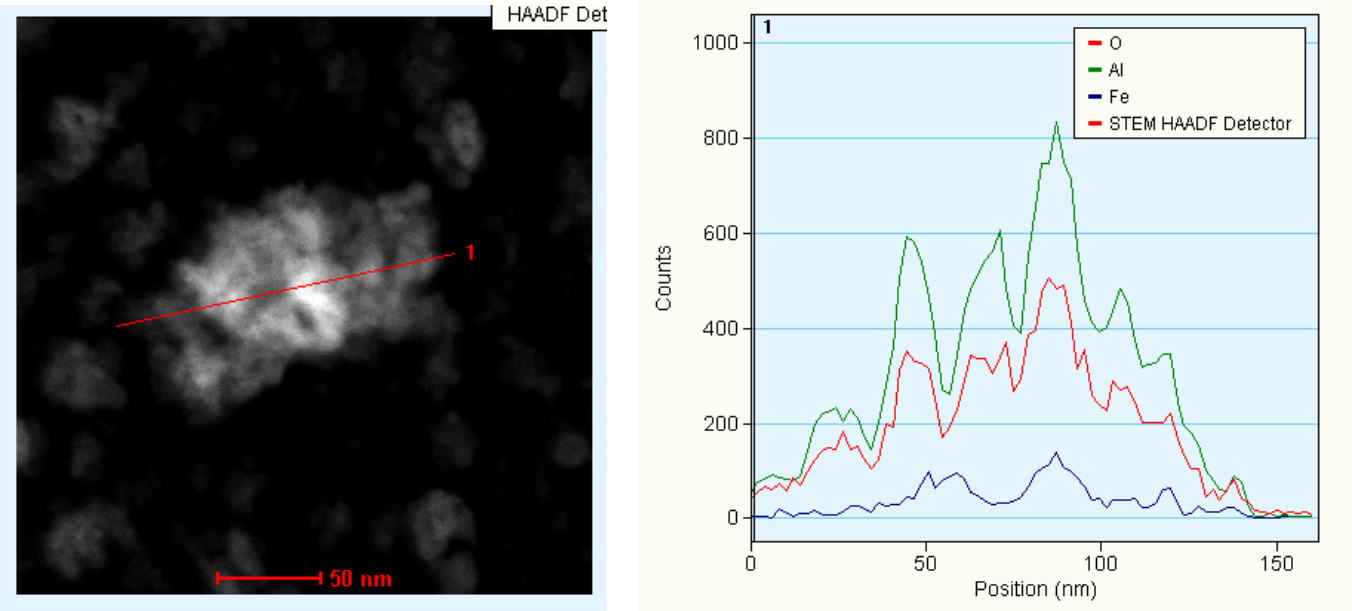

Figure 3. TEM image (left) and its associated energy dispersion (right) of elements oxygen, iron and alumina for 20FeA-A/E sample.

Crystallite diameters determined by XRD, TEM, and H_2 chemisorption are summarized in Table 2 (some of these data were reported in our first annual report). Crystallite sizes calculated from XRD and TEM are very similar and for two of the samples larger than those estimated from H_2 chemisorption. Smaller estimates from H_2 adsorption are expected, since iron clusters of $d < 3$ nm of which there could be many, cannot be detected by XRD but can nevertheless adsorb H_2, while TEM averages are based on distributions which weight more heavily the largest crystallites. The order of crystallite size for these three alumina-supported iron catalysts is 10FeA-W > 20FeA-A/E > 10FeA-A/E. These data establish that the nonaqueous evaporative deposition method produces supported iron catalysts of higher metal dispersion than the aqueous impregnation.

Table 2. Comparison of iron crystallite diameters determined by XRD, TEM, and H_2 chemisorption.

Samples	XRD (nm)	H_2 Chemisorption (nm)	TEM (nm)
10FeA-W	20.1	12.6	20
10FeA-A/E	6.0	6.2	5~10
20FeLaA-A/E	10.1	4.2	~10

C. CO-Temperature-Programmed Desorption (TPD) and Hydrogenation (TPH)

1. CO adsorption and TPD measurements on unsupported iron catalysts by Mass-spectrometer

About 300 mg of catalyst was reduced at 450ºC for 12 h at 1ºC/min, and then purged in He at 430ºC for 30 min. After cooling to RT, CO was introduced to the catalyst for 12 h. The sample was then cooled in CO with a dry ice/acetone bath to –84ºC and purged in He for 30 min to remove physically adsorbed CO; it was then heated to 750ºC at 15ºC/min. The CO in this process was determined by mass spectrometry. The procedure is shown schematically in Fig. 4.

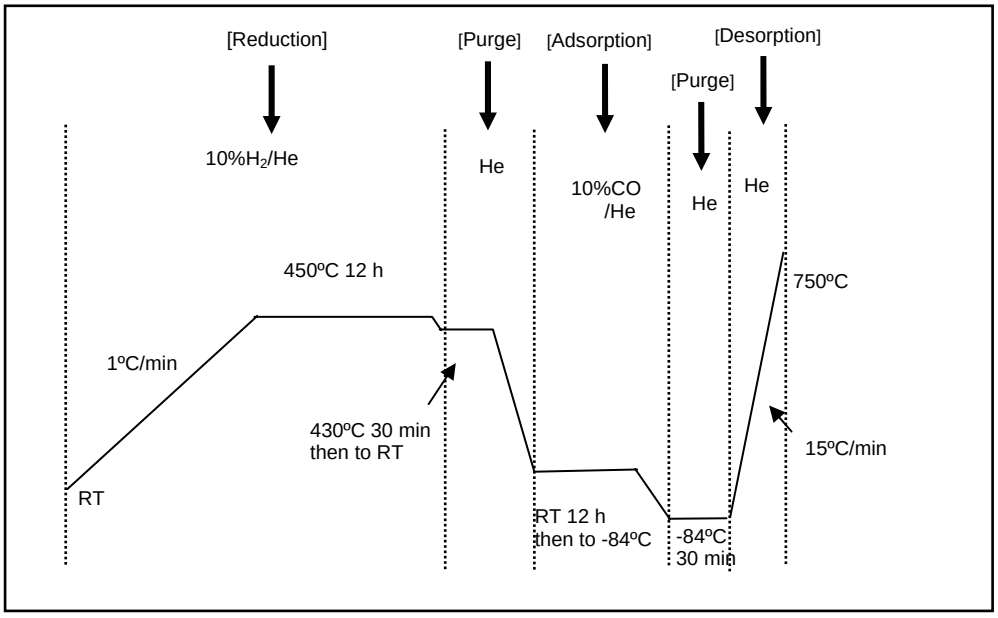

Figure 4. Schematic of CO adsorption/desorption procedure with mass-spectrometry.

During thermal desorption of CO from a stepped Fe (111) surface at low exposures, two desorption maxima (peaks) are observed at ~380 K (α-CO) and at ~700 K (assumed to be a broad β-peak). [3, 4] At higher exposures, the α-peak is accompanied by a shoulder at the lower temperature side. The α-CO from the iron surfaces can be ascribed to molecularly-adsorbed CO of the linear type and the β-CO from the iron surfaces is assigned to dissociated CO. Other researchers observed these two thermal desorption peaks at different temperatures. For example, U. Seip et. al. [5] reported peaks at 420 K and 820 K, respectively, and C. E. Bartosch et. al. [6] observed peaks at 400 K and 750 K. Thermal desorption spectroscopy of CO from Fe (110) was studied by K. Ueda et. al; [7] two peaks at 293 K and 723 K were observed.

We prepared unsupported Fe catalysts with a 1 wt% alumina structural additive and 1 wt% K or 1 wt% Pt promoters, for CO-TPD experiments. CO adsorption at RT and CO-TPD measurements on 99FeA series catalysts were carried out *in situ* by mass spectrometry.

Figures 5-7 show the CO-TPD patterns of 99FeA, 99FeA-Pt, and 99FeA-K samples, respectively. Table 3 summarizes peak temperatures and their assignments. Desorption peaks below 298 K for all three reduced samples are probably due to weakly physically and molecularly-adsorbed CO. Two other typical desorption peaks observed for 99FeA and 99FeA-Pt CO-TPD at 353-383 K and 629-715 K are associated with molecularly-chemisorbed CO and dissociated CO respectively, similar to those observed for the Fe single crystal surfaces, although the peak temperatures for dissociative adsorption are generally lower for the 99% Fe relative to single crystal surfaces. However, two additional peaks for the 99FeA-K sample are observed at higher temperatures than for 99FeA, i.e. 182ºC (455 K) and 571ºC (844 K), suggesting that CO adsorbs on 99FeA-K sample more strongly than 99FeA sample. These peaks are attributed to Fe-K-CO interfacial sites.

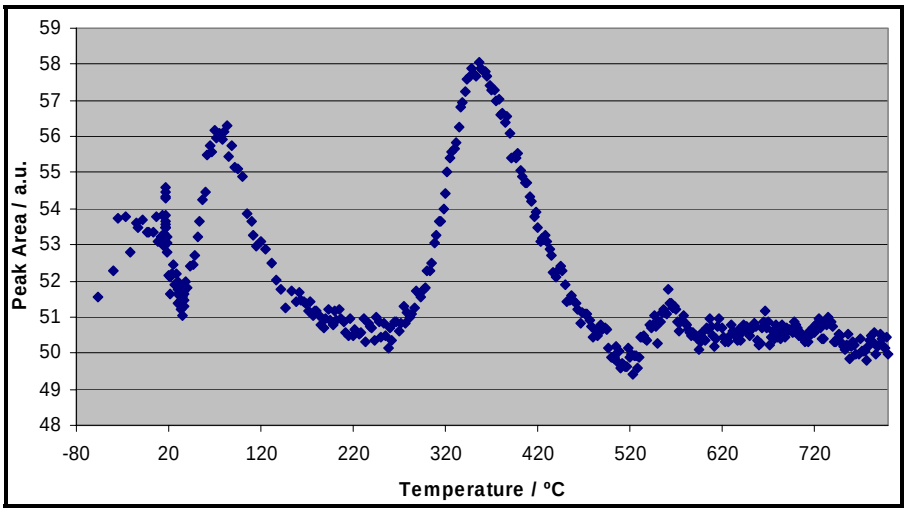

Figure 5. CO-TPD pattern of 99FeA sample.

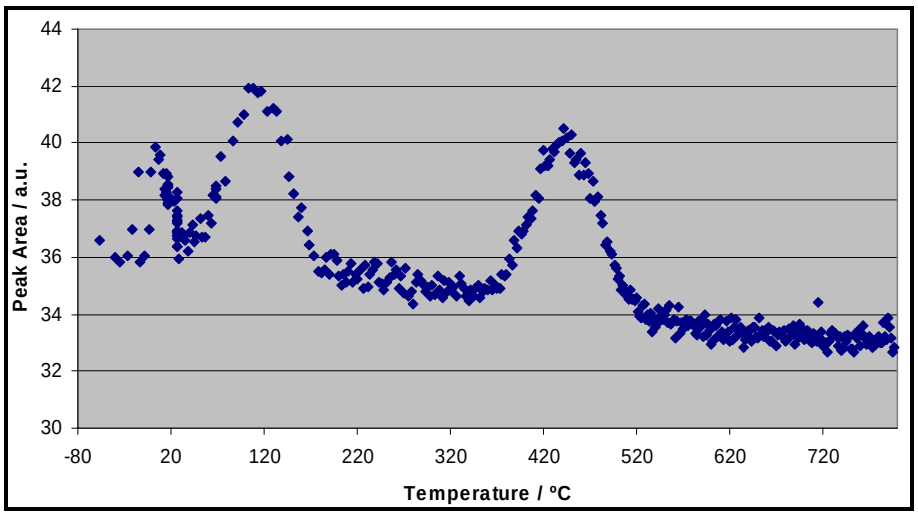

Figure 6. CO-TPD pattern of 99FeA-Pt sample.

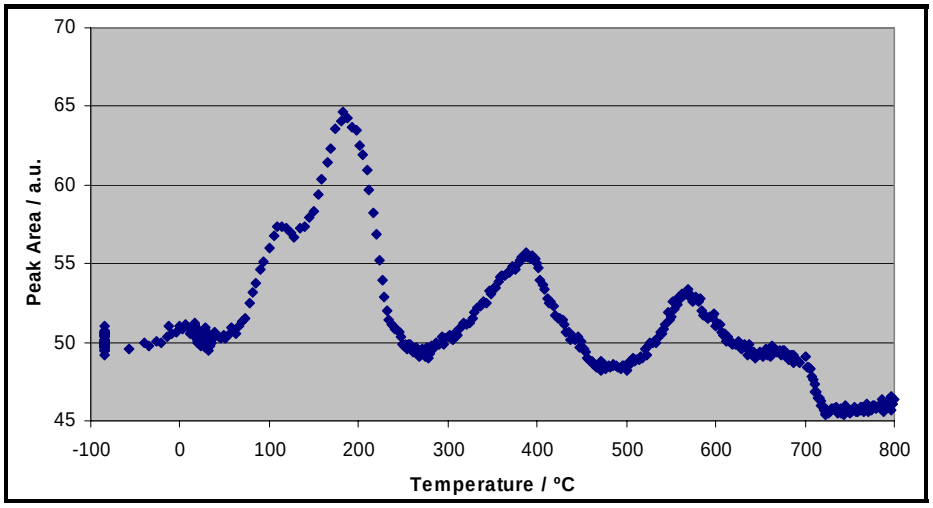

Figure 7. CO-TPD pattern of 99FeA-K sample.

Table 3. Summary of thermal desorption peaks

Samples	Peak temperatures, ºC (K)	Ascription
99FeA	15 (288)	Weak physically molecularly-adsorbed CO
	80 (353)	Molecular chemisorbed linear CO
	356 (629)	Dissociated CO
99FeA-Pt	10 (283)	Weak physically molecularly-adsorbed CO
	110 (383)	Molecular chemisorbed linear CO
	442 (715)	Dissociated CO
99FeA-K	6 (279)	Weak physically molecularly-adsorbed CO
	114 (387)	Molecular chemisorbed linear CO
	182 (455)	Molecularly-adsorbed CO of the linear type on Fe-K sites
	395 (668)	Dissociated CO on iron sites
	571 (844)	$K_x(CO)_y$ species

It is worth noting that CO adsorption on unsupported Fe, FePt, and Fe K catalysts was carried out at mainly room temperature (see Experimental section). CO dissociation takes place at this mild condition and the fraction of dissociatively-adsorbed CO is roughly 0.5 estimated by the peak areas. This suggests that this step is facile in FTS process which takes place at much higher temperatures; hence CO dissociation is unlikely to be a slow or rate-determining step at typical FT reaction temperatures.

Figure 8 shows CO-TPD patterns following adsorption at three different temperatures (25, 50, and 100ºC) on the 99FeA catalyst. CO-TPD experiments were stopped at 450ºC. The amounts of adsorbed CO of both types decrease with increasing adsorption temperature. Less CO adsorbed at higher temperatures indicates that CO adsorption is increasingly reversible with increasing adsorption temperature, a phenomenon typical of chemisorption on metals.

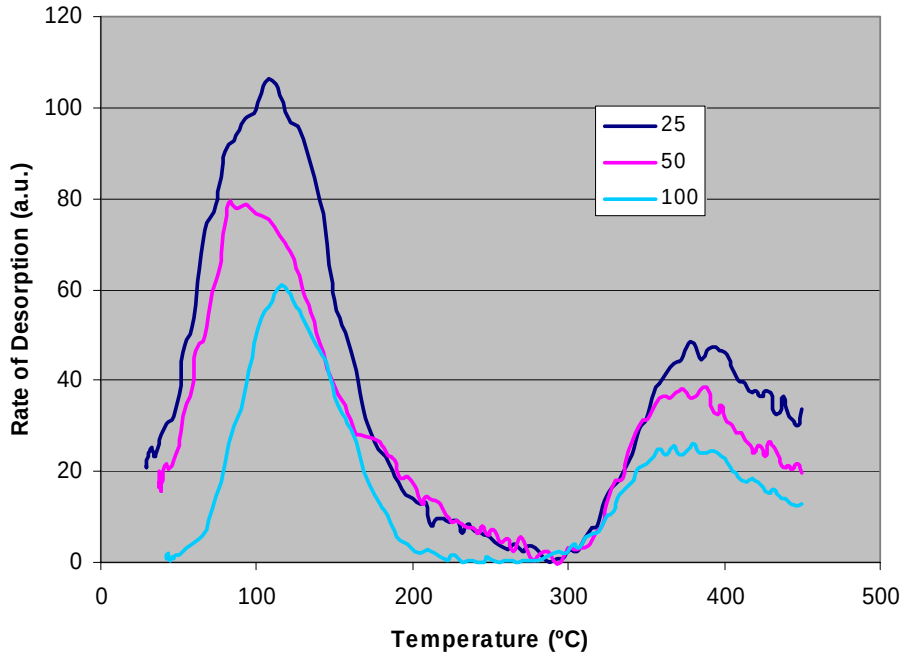

Figure 8. CO-TPD patterns at Different Adsorption Temperatures on 99FeA.

2. TPH measurements by mass-spectrometry

Two sets of C hydrogenation rate versus time were conducted on Fe samples (see Fig. 9):

(1) Isothermal hydrogenation of carbonaceous adsorbed species: The sample was pretreated in H_2 at 450ºC and 1 atm for 12 h. After decreasing the reaction temperature to 200ºC in helium, the reactant mixture of 25% CO/H_2 was then admitted for 10 min, followed by a purge in helium for 8 min. H_2 was then introduced immediately onto the catalyst and methane evolved was detected by a quadrupole mass-spectrometer.

(2) TPH: After isothermal hydrogenation for 2 h, the temperature was increased from 200ºC to 800ºC at 12ºC/min in H_2 to obtain a TPH spectrum.

Figure 10 shows the isothermal hydrogenation spectra for removal of carbonaceous species from the three 99FeA series samples. Only one methane formation peak is observed, which reaches a maximum at about 500-800 s, after which methane concentration levels out at a nonzero value after about 3500-4000 s. The observation of only one methane peak is different from results reported for supported iron catalysts in literature.[8] Because of the short exposure to syngas and the mild conditions for removal (50-70°C below typical reaction temperatures), the

methane is probably associated with hydrogenation of atomic surface carbon. Carbon hydrogenation rate increases in the order Fe, FePt, FeK.

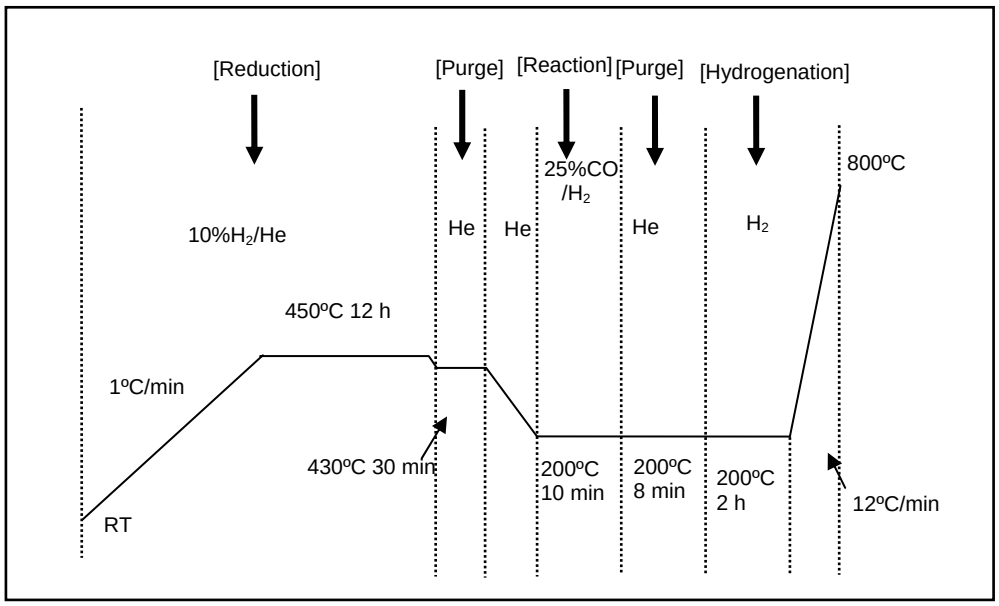

Figure 9. Schematic of TPH procedure with mass-spectrometry.

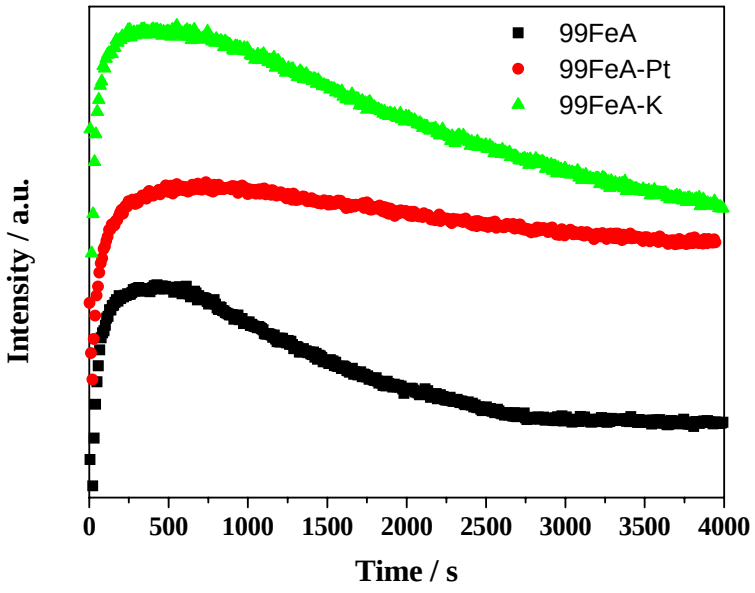

Figure 10. Isothermal hydrogenation spectrum of carbonaceous species of 99FeA sample at 200°C.

The results in Figure 10 show that reaction kinetics of carbon hydrogenation on Fe are readily studied under these mild reaction conditions. Kinetic parameters will be obtained by varying the exposure time (and thus carbon coverage from about 0.2 to 0.5), hydrogen partial

pressure, and reaction temperature. Kinetics of CO dissociation will be obtained by varying the same parameters followed by complete removal of carbon by temperature programmed hydrogenation (TPH). Based on a H_2 chemisorption uptake of 97 μmol/g, roughly 15% of a monolayer of C is removed from the 99FeA catalyst in this experiment.

Figure 11A contains TPH spectra of 99FeA, 99FeA-Pt, and 99FeA-K samples. TPH spectra should show methane evolution rate due to reaction of carbon with H_2. However, its y-axis is intensity of signal of mass-spectrometer because of lack of calibration data. An enlarged section which includes peaks at low temperatures is shown in Figure 11B. The intensity of peaks at high

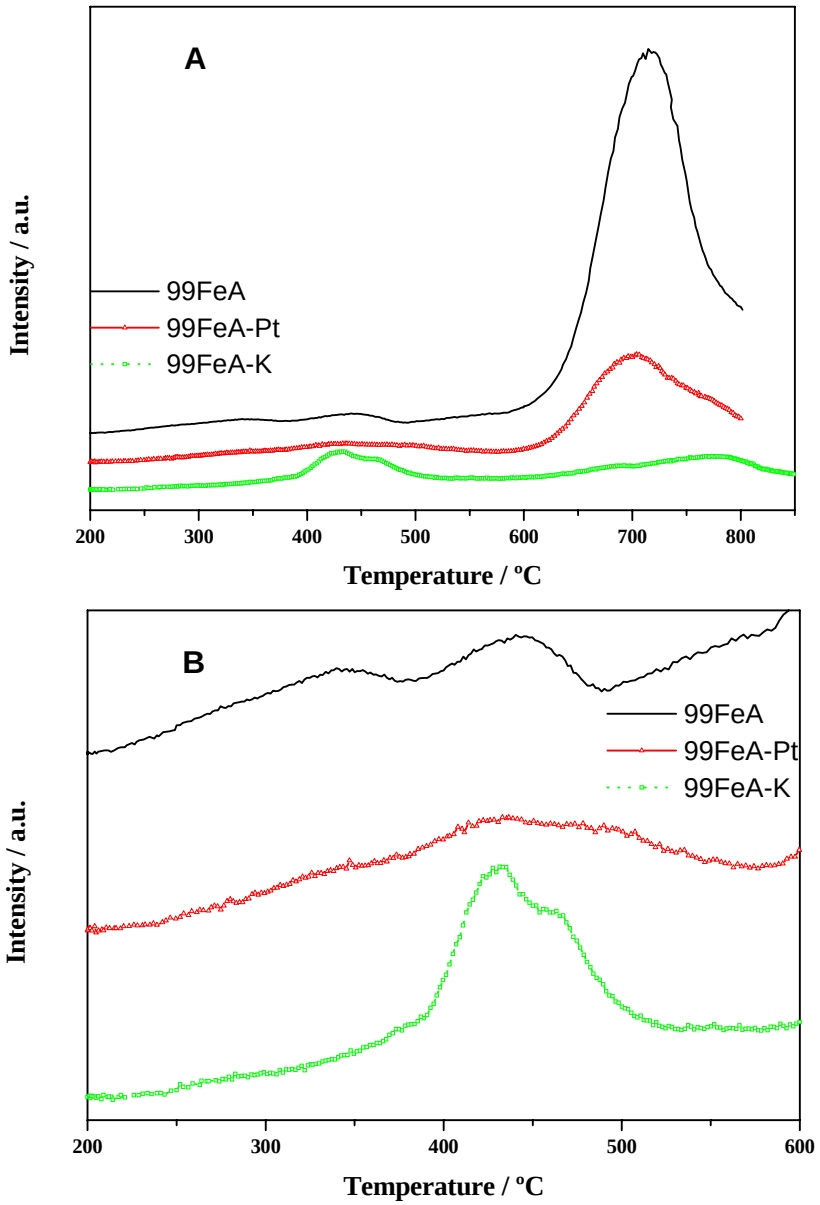

Figure 11. (A) TPH spectra of 99FeA series samples; (B) Enlarged section of temperature period between 200 and 600ºC.

temperature for 99FeA sample is the highest for 99FeA-Pt medium and lowest for 99FeA-K. A method for quantitative analysis of overlapping TPH peaks for unpromoted and K-promoted Fe FT catalyst was reported by Eliason and Bartholomew.[9] Their spectra were fitted with Gaussian curves to yield up to seven peaks, designated as α_1, α_2, β, γ_1, γ_2, δ_1 and δ_2. Figures 12-14 show deconvoluted TPH spectra for the three unsupported samples of this study. The dashed line is the sum of the individual peaks directly overlaying the measured spectrum in each case. The optimized analysis for the 99FeA and 99FeA-Pt samples yielded seven peaks and the analyses for the 99FeA-K sample yielded eleven peaks. Table 4 lists temperatures associated with each H_2-TPSR peak maximum for these three catalysts. α, β, γ, and δ species are assigned to adsorbed atomic carbon, amorphous surface methylene chains or films, bulk iron carbide, and graphitic carbon. α_1 and α_2 refer to atomic carbons on different sites. Four additional individual peaks for the 99FeA-K (compared with 99FeA) suggest that there are unique adsorption sites which may be attributed to Fe-K interfacial sites.

Comparison of the spectral areas in Fig. 11A shows that about 4 and 10 times less carbon is deposited on 99FeA-Pt and 99FeA-K compared to 99FeA; thus, Pt and K promoters are effective in keeping the surface clean during reaction by facilitating gasification of carbon species. The large high-temperature peaks observed in the spectrum for 99FeA (Fig. 12), assigned to iron carbide and δ–carbon, comprise a large fraction of the spectral area, indicating that mostly inactive forms of carbon are deposited on the unpromoted Fe catalyst during a very short period of reaction under very mild conditions (only 10 minutes at 200°C). By contrast, of the relatively small quantity of carbon species deposited during reaction on the surface of 99FeA-K (Fig. 14), about half of are active species, easily gasified with H_2 at temperatures below 500ºC.

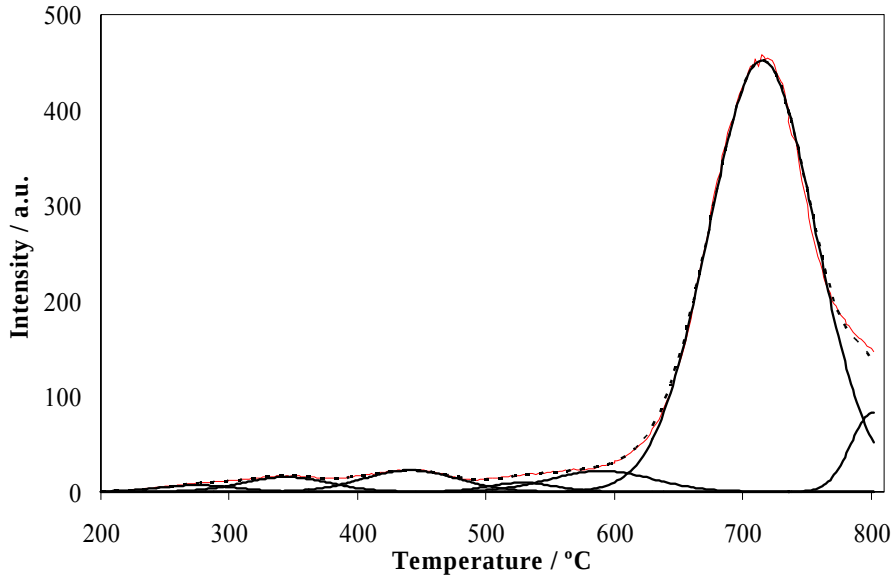

Figure 12. TPH spectra showing individual peak contributions from the carbon species on 99FeA.

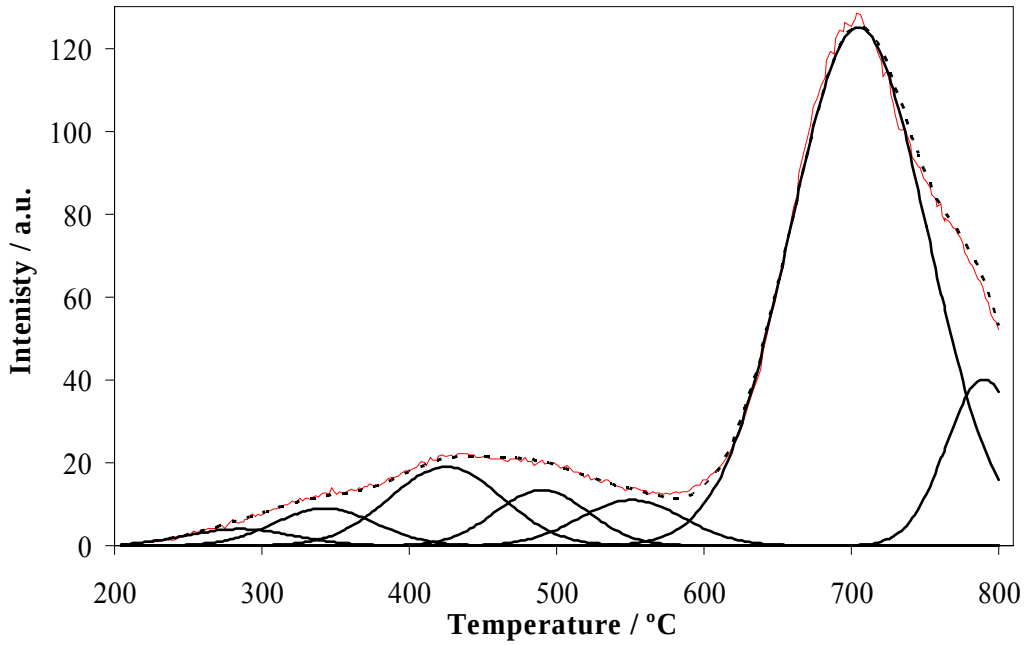

Figure 13. TPH spectra showing individual peak contributions from the carbon species on 99FeA-Pt.

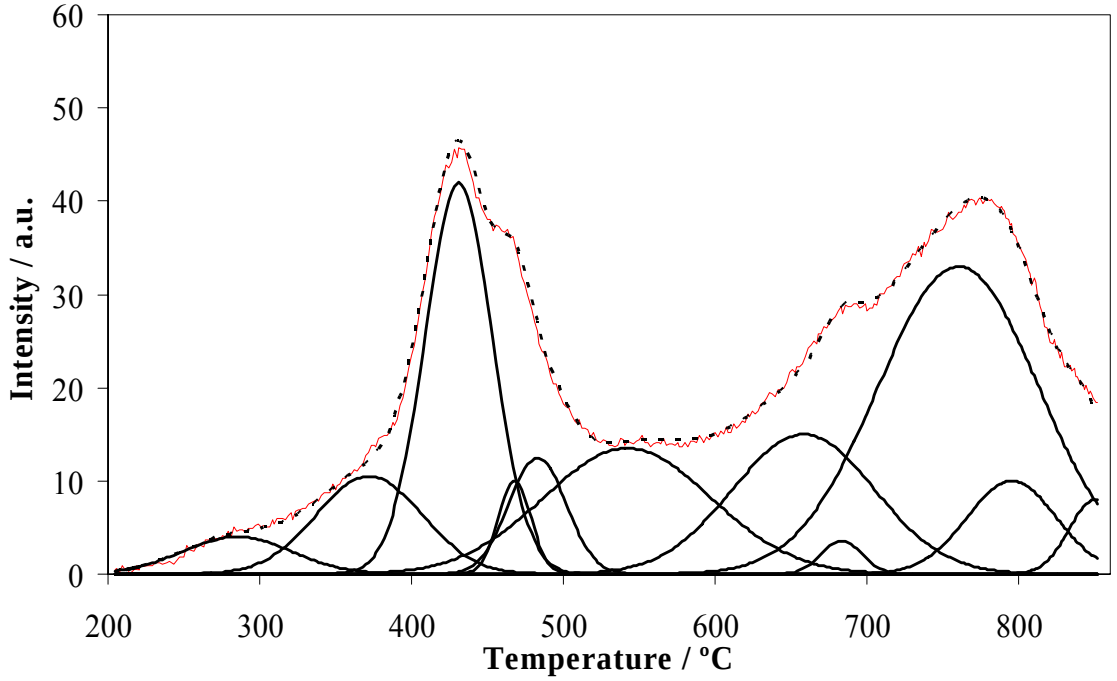

Figure 14. TPH spectra showing individual peak contributions from the carbon species on 99FeA-K.

Table 4. Peak temperature assignments for TPH of carbonaceous species on 99FeA series .

Samples	Peak Temperature (ºC)						
	Carbidic		Amorphous	Carbide		Graphitic	
	α_1	α_2	β	γ_1	γ_2	δ_1	δ_2
99FeA	275	344	441	528	590	715	801
99FeA-Pt	285	343	425	490	551	705	790
99FeA-K	285	372	431 468*	483 542*	658 683*	760	795

* The carbon species may be associated with Fe-K sites.

3. TPR measurements on supported iron catalysts by TGA and MS

CO adsorption on and desorption from Al_2O_3-supported samples were studied using TGA. A catalyst sample of 40-50 mg was charged to the TGA pan and first reduced in 10% H_2/He as follows: 1ºC/min from room temperature to 120ºC, hold at 120ºC for 1 h, 1ºC/min to 400ºC, and hold at 400ºC for 12 h. After reduction, H_2 flow was discontinued, while He flow was continued for 30 min at 400ºC to desorb H_2. The sample was cooled to room temperature in flowing N_2. CO was introduced to the sample at room temperature by flowing 10% CO/He for 1 h. Finally, the sample was exposed to pure He while temperature was increased linearly to desorb CO.

Figure 15 shows the CO-TPD/TGA spectrum for a 20FeA-A/E sample. Consistent with unsupported iron samples, two CO desorption peaks assigned to molecularly-adsorbed and dissociated CO can be seen in Figure 15. However, the peak for recombination of the predissociated CO is significantly shifted to lower temperature (280ºC). This indicates that the C-Fe bond is weaker than that formed on 99FeA series samples.

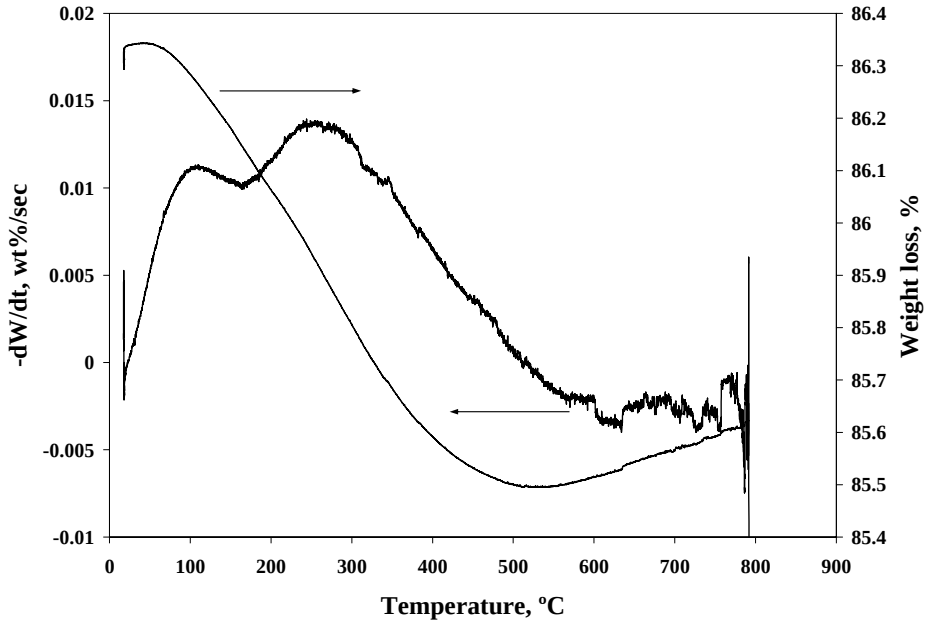

Figure 15. CO-TPD/TGA pattern of 20FeA-A/E sample.

In situ CO adsorption and TPD measurements were carried out on a series of alumina supported iron catalysts, denoted as 20FeLaA (20 wt% Fe/6 wt% La_2O_3/Al_2O_3), 20FeKLaA (20 wt% Fe/1 wt% K/6 wt% La_2O_3/Al_2O_3), and 20FePtLaA (20 wt% Fe/1 wt% Pt/6 wt% La_2O_3/Al_2O_3) using our TPD/TPR system with mass spectrometric analysis. Figure 16 shows the CO-TPD patterns of these three catalysts following adsorption at 25ºC, cooling to -83ºC, and ramping temperature linearly to 730ºC. Two CO desorption peaks are observed at –9 and 83ºC for the 20FeLaA catalyst, and at –15 and 75ºC for the 20FePtLaA catalyst. The first peak for both samples is due to weak molecular CO desorption (indicating physically adsorbed CO), while the second peak is due desorption of chemisorbed CO molecules. The absence of a peak at higher temperatures (e.g. around 250-400ºC) indicates that CO dissociation does not occur on the 20FeLaA and 20FePtLaA catalysts after CO adsorption at room temperature. CO desorption from the 20FeKLaA catalyst is more complicated than for 20FeLaA and 20FePtLaA samples.

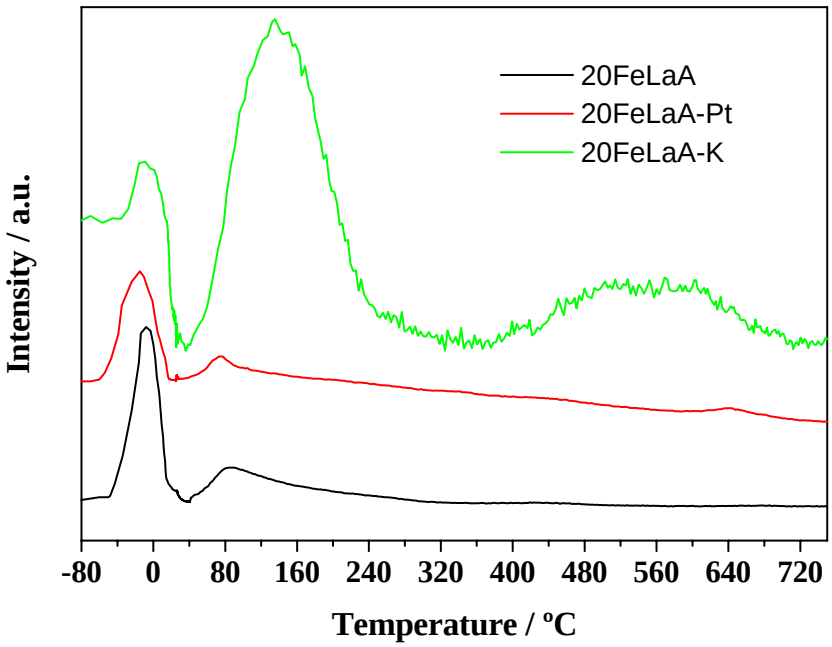

Figure 16. CO-TPD/MS patterns of 20FeLaA series samples.

The first CO-TPD peak for 20FeLaA-K located at -10ºC is probably due to desorption of physisorbed, molecular CO. The second peak with a maximum at 138ºC (significantly more intense and shifted to higher temperature relative to the 20FeLaA and 20FeLaA-Pt samples) is attributed to desorption of chemisorbed, molecular CO. The broad peak at 554ºC may be attributed to an overlap of peaks due to recombination of adsorbed C and O atoms located (1) on metal sites which desorb at lower temperatures and (2) on sites near to surface K which desorb at higher temperatures, since they are more strongly bound. The observation of the high-temperature desorption and its assignment to recombination of predissociated CO are consistent with observations from previous literature that surface K increases the Fe-C bond strength, thus enhancing CO dissociation. Thus, the supported 20FeKLaA catalyst behaves similarly to the

unsupported 99FeKA catalyst in dissociating CO at low temperature. However, the inability of the supported 20FeLaA catalyst to dissociate CO at RT is qualitatively and quantitatively different than for unsupported 99FeA. TPD measurements following adsorption at progressively higher temperatures are important, since at higher temperatures, CO dissociation is more likely to occur on the La-Al_2O_3-supported catalysts.

The differences in the TPH spectra obtained by TGA and by mass spectrometry for alumina-supported Fe are very striking. Further study is needed to understand the reasons for these differences. They may relate to (1) differences in the catalyst support and catalyst preparation, (2) fundamental differences in the method of measurement, e.g. the TGA method based on weight loss of the sample may include desorption of water and CO_2 while the MS method would not include either effect.

4. TPH measurements on supported iron catalysts by TGA

Procedures were as follows:

1) H_2 reduction: About 30~40 mg samples were put on a TGA pan and treated in 10% H_2/He (20 sccm H_2 in 180 sccm He), ramped at 1ºC/min to 400ºC, held for 12 h, and then cooled to 380ºC in pure He and held for 30 min (see Fig. 17).

2) CO hydrogenation: Samples were cooled down to 200ºC in pure He with ramping rate of 40ºC/min, and then reacted in CO/H_2/He (1:4:16) at 200ºC for 5 min, then purged in He for another 5 min. Samples were cooled to room temperature quickly (see Fig. 17).

3) TPH. Following these pretreatments, samples were exposed to 10% H_2/He while ramping to 800ºC at 5ºC/min (see Fig. 17).

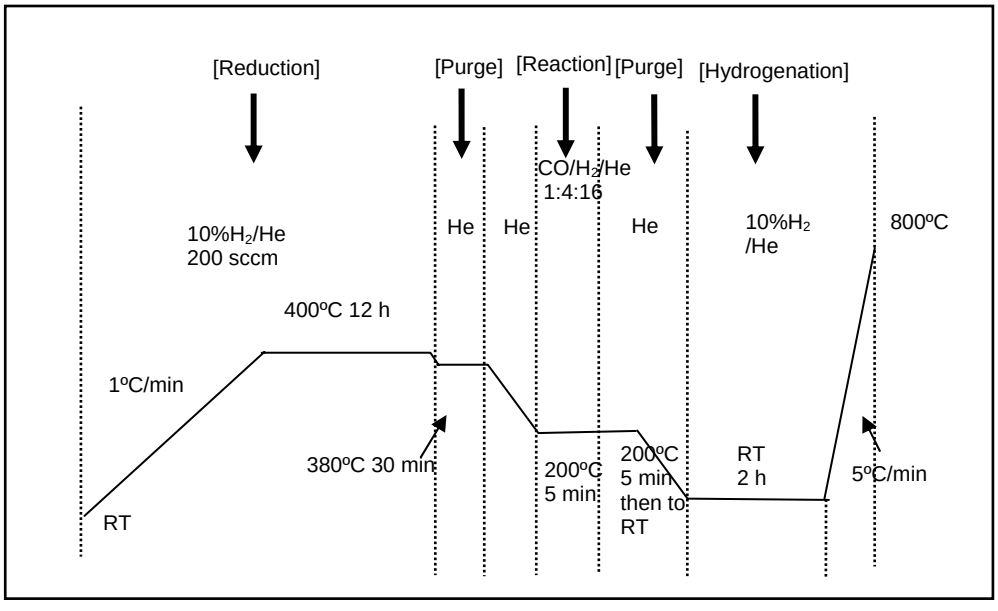

Figure 17. Schematic of TPH procedure by TGA.

TPH experiments were carried out following FT reaction for the three alumina-supported 10% and 20% Fe catalysts using TGA. Figures 18-20 show the weight changes as a function of the temperature and associated TPH spectra. The weight increase (weight change curve) at reaction temperature below 200ºC for all three samples is probably due to hydrogen adsorption on iron crystallites. Several overlapping derivative peaks are observed above 200ºC.

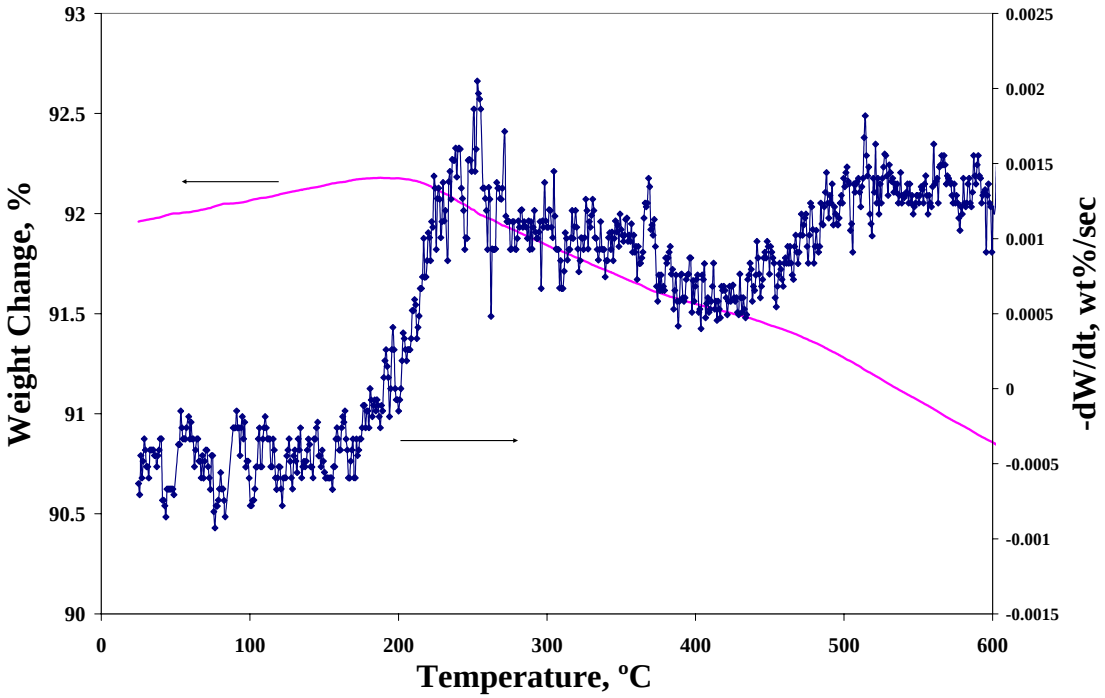

Figure 18. Temperature-programmed hydrogenation of carbonaceous species on 10FeA-W.

Quantities of carbonaceous species were roughly estimated from weight change curves and used to calculate monolayer carbon equivalents based on hydrogen chemisorption data. Corresponding deconvoluted spectra are shown in Figures 21-23; a TPH spectrum obtained by mass spectrometry for the 20% Fe/alumina is shown for purposes of comparison in Fig. 24. Observed peak temperatures and their assignments are listed in Table 5. Table 6 lists the area under each curve in terms of carbon monolayer equivalents based on iron metal surface area. The corresponding percentage compositions of carbon species are given in Table 7. The carbon monolayer equivalent of α-carbon (reactive atomic carbon) is highest for 10FeA-W. 10FeA-A/E and 20FeA-A/E have the same carbon monolayer equivalents of α-carbon. The order of the fractional compositions for various carbon phases for 10FeA-W is $\gamma > \beta > \alpha > \delta$; for 10FeA-A/E is $\gamma > \delta > \beta > \alpha$, and for 20FeA-A/E is $\delta > \gamma > \alpha \cong \beta$. The results indicate that 10FeA-A/E and 20FeA-A/E have large fractions of inactive carbon species on the surface after FT reaction. Unfortunately, the TPH experiments had to be terminated at 600ºC because of equipment limitations and hence the fraction of graphitic species should be larger than is shown in Table 6.

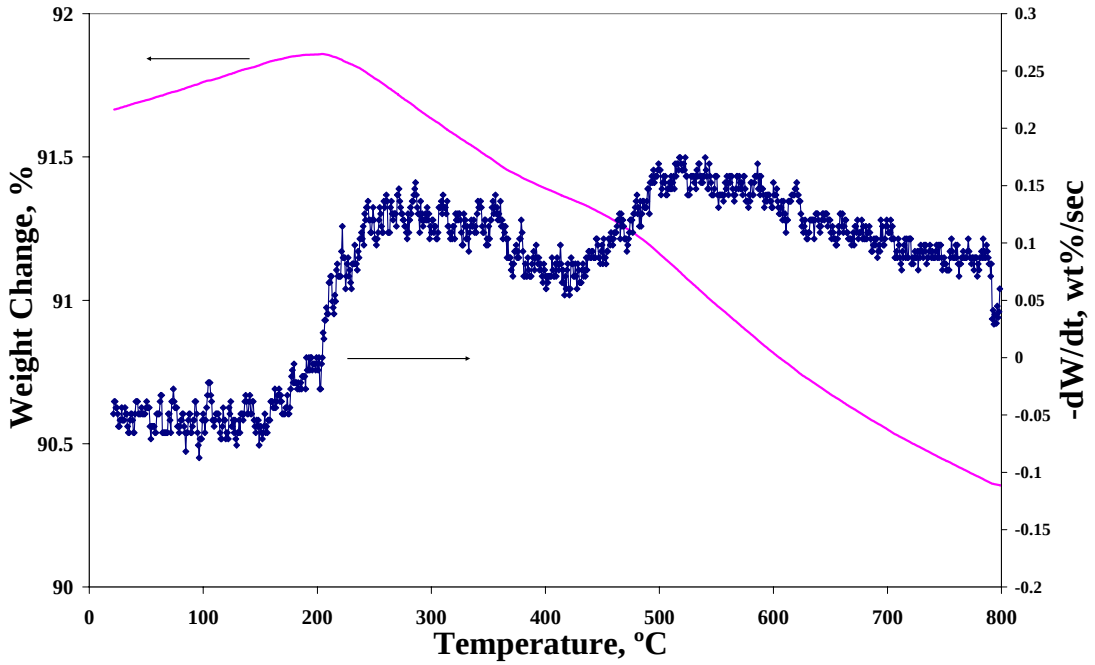

Figure 19. Temperature-programmed hydrogenation of carbonaceous species on 10FeA-A/E .

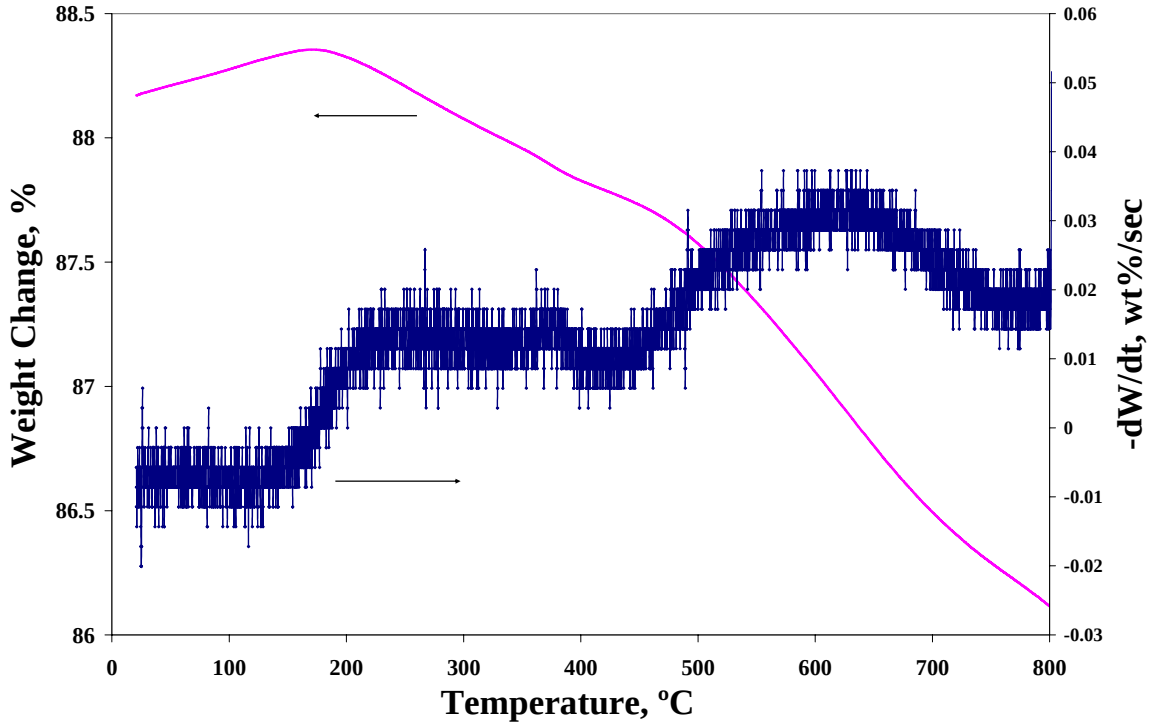

Figure 20. Temperature-programmed hydrogenation of carbonaceous species on 20FeA-A/E .

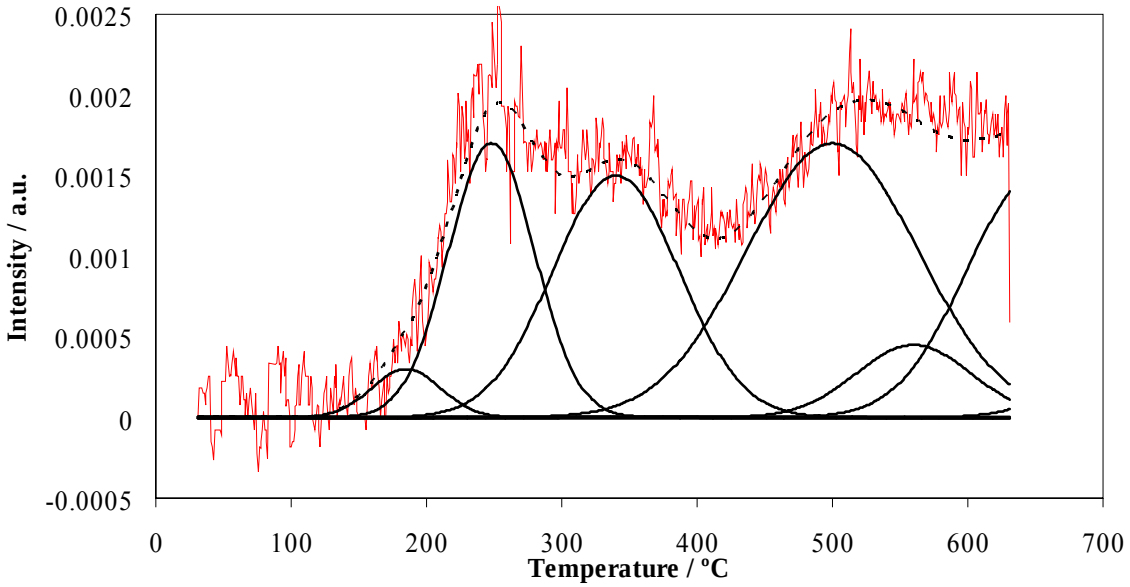

Figure 21. TPH spectra showing individual peak contributions from various carbon species for 10FeA-W.

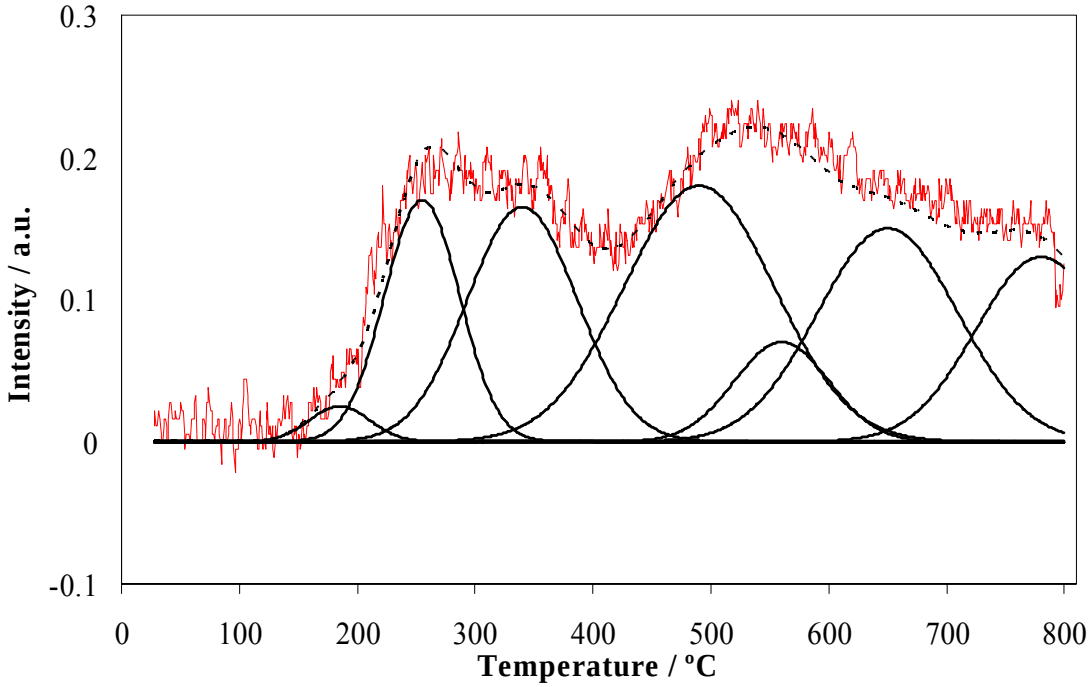

Figure 22. TPH spectra showing individual peak contributions from various carbon species for 10FeA-A/E.

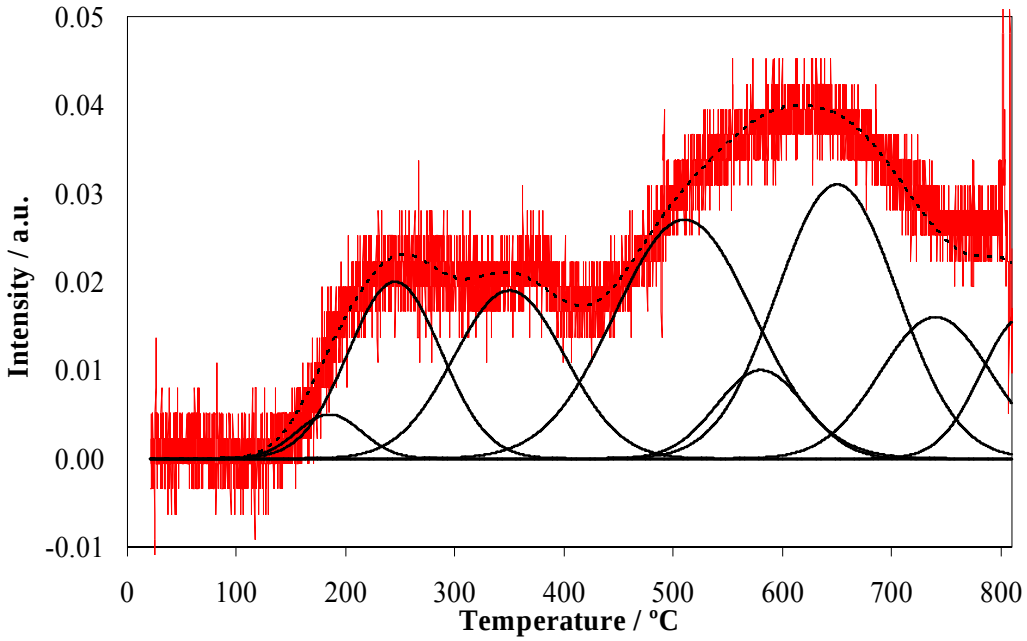

Figure 23. TPH spectrum obstained by TGA showing individual peak contributions from various carbon species for 20FeA-A/E.

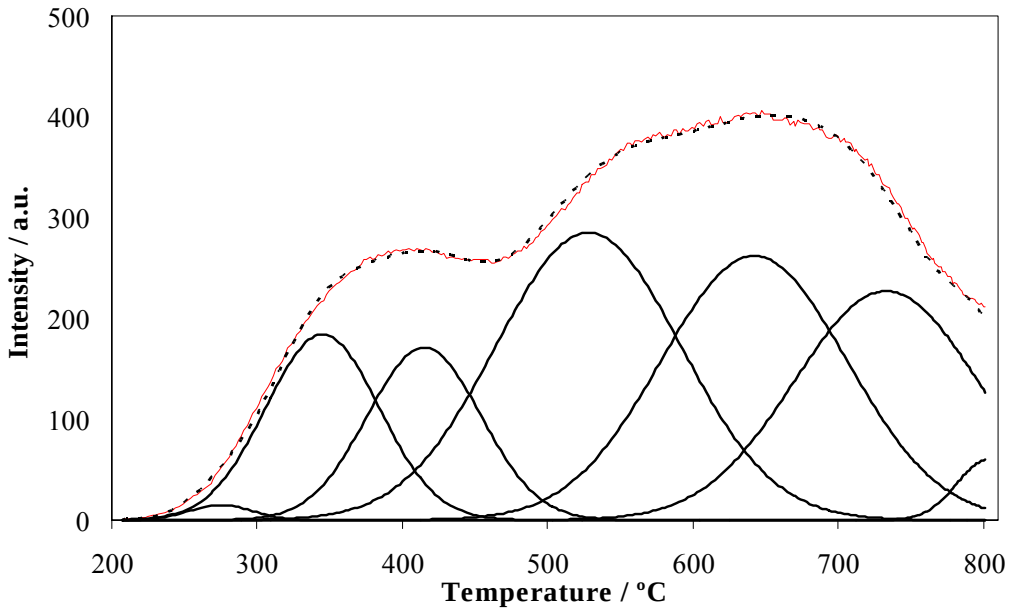

Figure 24. TPH spectrum obtained by TPSR/MS showing individual peak contributions from the various carbon species of 20FeA-A/E sample.

Table 5. Results of Temperature-Programmed Surface Reaction (TPH) of H_2 with carbonaceous species on supported catalysts

Samples	Peak Temperature (°C)						
	Carbidic		Amorphous	Carbide		Graphitic	
	α_1	α_2	β	γ_1	γ_2	δ_1	δ_2
10FeA-W	185	248	340	500	560	650	780
10FeA-A/E	185	255	340	490	560	650	780
20FeA-A/E	185	245	350	510	580	650	740

Table 6. Fractional compositions for various carbon phases on supported catalysts

Samples	Carbidic		Amorphous	Carbide		Graphitic	
	α_1	α_2	β	γ_1	γ_2	δ_1	δ_2
10FeA-W	0.03	0.19	0.25	0.38	0.06	0.10	0.00
10FeA-A/E	0.02	0.13	0.19	0.28	0.07	0.21	0.11
20FeA-A/E	0.02	0.13	0.15	0.25	0.06	0.25	0.11

Table 7. Monolayer carbon equivalents of peak areas on supported catalysts

Samples	Carbidic		Amorphous	Carbide		Graphitic	
	α_1	α_2	β	γ_1	γ_2	δ_1	δ_2
10FeA-W	0.327	2.071	2.725	4.142	0.654	1.09	0
10FeA-A/E	0.0424	0.2756	0.4028	0.5936	0.1484	0.4452	0.2332
20FeA-A/E	0.0352	0.2288	0.264	0.44	0.1056	0.44	0.1936

For comparison's sake, TPH was carried out on a 20FeA-A/E sample using the TPD/MS system. The TPH spectrum and the corresponding deconvoluted spectra are shown in Figure 24. The distribution of carbonaceous species is very similar to the result obtained by TGA (Fig. 23); however, larger amounts of the carbide species were determined from the TPD/MS results.

D. Activity tests

FTS activity of alumina-supported iron catalysts were carried out in a fixed-bed FTS reactor. CO conversion versus time on stream for 10FeA-W, 10FeA-A/E, and 20FeA-A/E catalysts is plotted in Fig. 25. CO conversion is higher for the 10FeA-W catalyst than for 10FeA-A/E and 20FeA-A/E catalysts. This order of activity correlates with the order of monolayer carbon equivalents of carbidic species. Another reason for the higher activity of the 10FeA-W catalyst can be attributed to its larger crystallite diameter and hence lower extent of metal cluster-support interaction and/or oxidation; these complications would be more pronounced in the 10FeA-A/E and 20FeA-A/E catalysts because iron crystallite sizes in these catalysts are very small (< 5 nm). In fact, researchers [10] have reported that the FTS activity of iron catalysts is lower if iron

crystallite size is less than 5 nm. The 10FeA-A/E exhibits highly stability over one week. The selectivity of C_{2+} is up to 86% for the three samples (see Fig. 26).

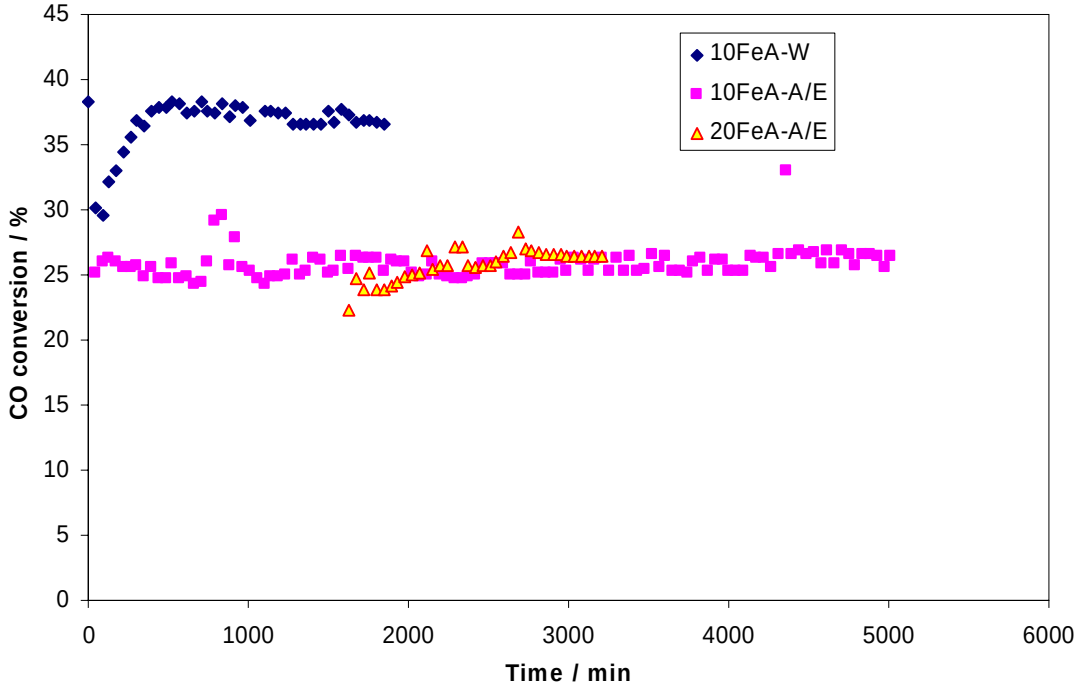

Figure 25. CO conversion plotted as time on stream (250ºC, 10 atm, $H_2/CO = 2$, SV: 3000 h^{-1}).

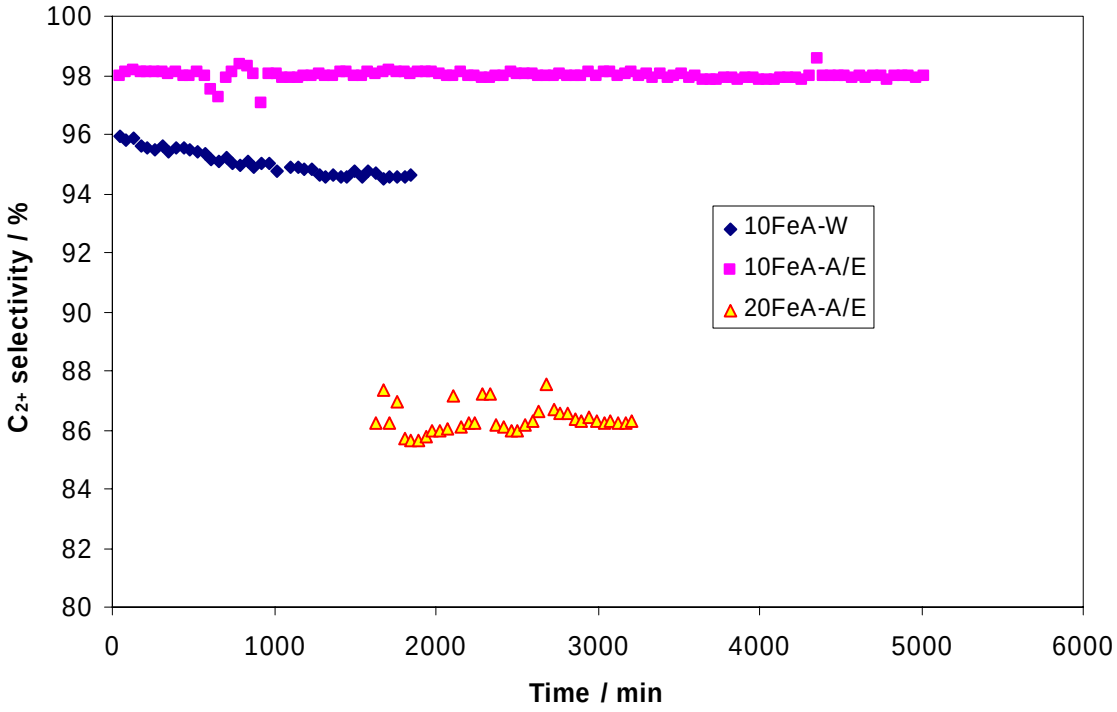

Figure 26. C_{2+} selectivity plotted as time on stream (250ºC, 10 atm, $H_2/CO = 2$, SV: 3000 h^{-1}).

E. Results of Statistically Designed for Determining Kinetic Constants for an FTS Reaction Model

Using our Berty Reactor System (whose schematic was given in last year's report), we obtained optimized raw kinetic data on supported Fe catalyst that will be used to validate our final mechanistic model. The experimental conditions were obtained using a sequential design approach utilizing a response surface design based on D-optimality. The rate expression used was a Langmuir-Hinshelwood (LH) type rate expression

$$r_{C_{2+}} = \frac{A\, P_{CO}^{0.67}\, P_{H_2}^{0.83}}{\left(1 + D\, P_{CO}^{0.67} P_{H_2}^{0.33}\right)^2} \qquad (1)$$

obtained from the mechanistic sequence with carbon hydrogenation and hydroxyl radical recombination as the rate determining steps.

	$CO + \mathbf{S}$	$\leftrightarrow$	$CO\text{–}\mathbf{S}$		(2)
	$H_2 + 2\mathbf{S}$	$\leftrightarrow$	$2\ H\text{–}\mathbf{S}$		(3)
	$CO\text{–}\mathbf{S} + \mathbf{S}$	$\leftrightarrow$	$C\text{–}\mathbf{S} + O\text{–}\mathbf{S}$		(4)
	$C\text{–}\mathbf{S} + H\text{–}\mathbf{S}$	$\rightarrow$	$CH\text{–}\mathbf{S} + \mathbf{S}$	RDS	(5)
	$CH\text{–}\mathbf{S} + H\text{–}\mathbf{S}$	$\rightarrow$	$CH_2\text{–}\mathbf{S} + \mathbf{S}$		(6)
	$O\text{–}\mathbf{S} + H\text{-}\mathbf{S}$	$\leftrightarrow$	$OH\text{–}\mathbf{S} + \mathbf{S}$		(7)
	$2\ OH\text{–}\mathbf{S}$	$\rightarrow$	$H_2O + H\text{–}\mathbf{S} + \mathbf{S}$	RDS	(8)
or	$OH\text{–}\mathbf{S} + H\text{–}\mathbf{S}$	$\rightarrow$	$H_2O + 2\,\mathbf{S}$		(9)

D-optimal design (DOD) method is a proven tool for maximizing the quantity of useful data that can be obtained in the least number of experiments. The important steps in D-optimal design are shown schematically in Figure 27.

1. Collecting data.

Data were collected in blocks with one independent variable held constant, e.g. temperature is held constant within a block but varied from block to block. Blocking has the advantages of (a) allowing treatment of one less independent variable in each block and (b) enabling the experimental design to become more focused and efficient with each succeeding block. Steps 2 and 3 are repeated until the kinetic coefficients have been determined within an acceptable range of uncertainty.

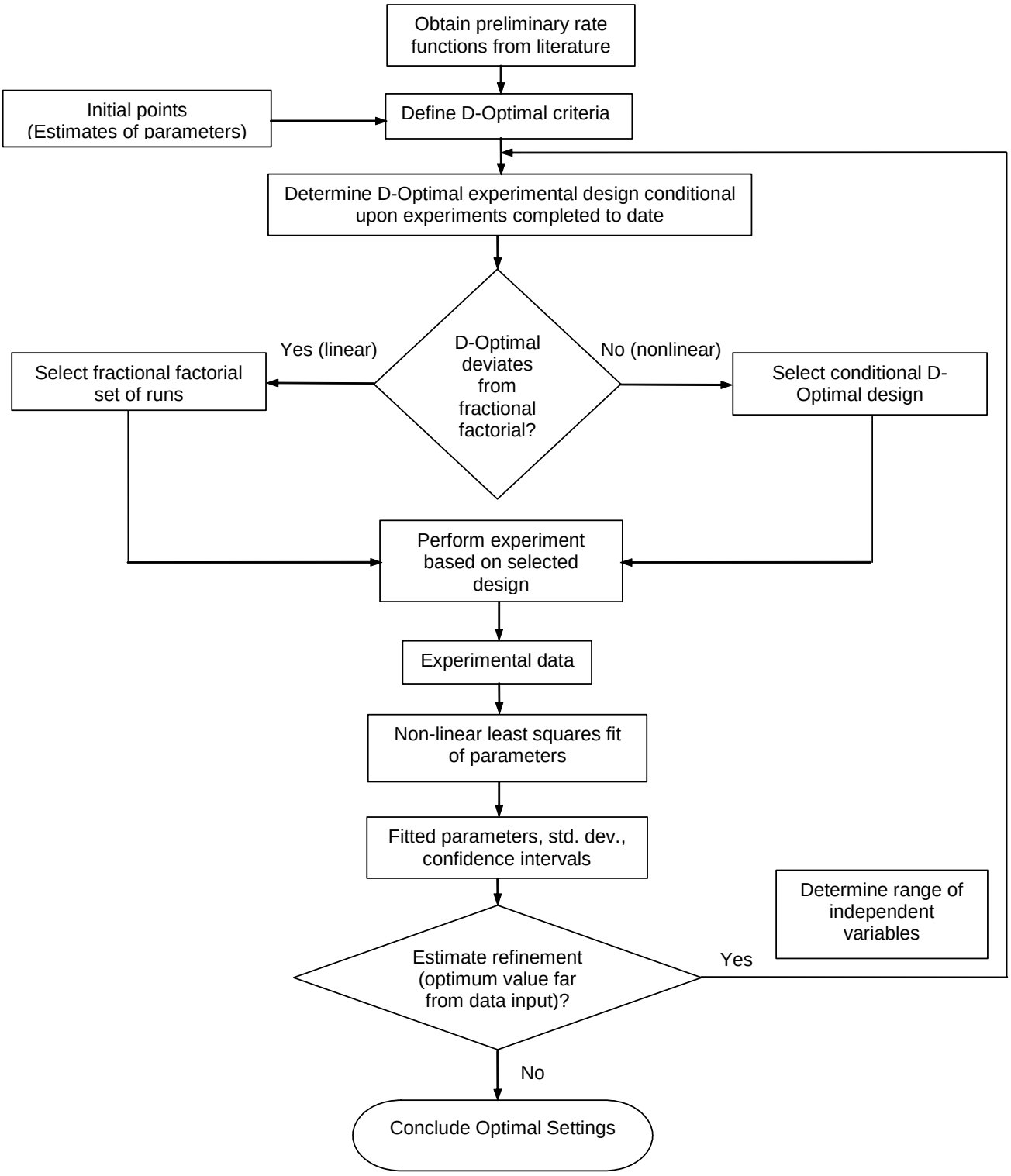

Figure 27. General Approach to D-Optimal Experimental Design.

2. Determining kinetic coefficients.

Once the determinant D has been maximized and collection of data is finished, the values of the kinetic coefficients, standard deviations and 95% confidence intervals were determined by nonlinear least squares regression of *all data*.

Initial set of five experimental points in terms of outlet partial pressures of carbon monoxide (CO) and hydrogen (H_2) as shown in the Table 8 below were chosen based on factorial experimental design. Then the kinetic constants were regressed based on results observed from these experimental points. D-optimality criterion was then applied resulting in another experimental condition. The experiment was then performed at this new experimental point with the data obtained added to the previous data and then regressing the kinetic constants. The process was continued until the values of the regressed constants and that of the D-optimality criterion asymptotes to a constant value. This process was carried out at two different temperature blocks (220^{o}C and 239^{o}C) respectively

Table 8. Experimental Run Number and Reactor Outlet Conditions at 220^{o}C.

Run #	P_{H2} (atm)	P_{CO} (atm)
1	9.4	3.9
2	9.5	3.9
3	3.8	4.0
4	3.8	0.9
5	10.1	0.7
6	9.8	4.0
7	10.0	0.7
8	3.9	0.9
9	9.9	4.0
10	9.6	4.0
11	10.1	0.8
12	3.8	0.9
13	10.1	0.7
14	3.8	0.9
15	9.9	4.0
16	3.8	0.9
17	6.9	2.4
18	3.7	4.1
19	9.7	3.9
20	9.8	3.8

Figure 28 shows the joint confidence interval plots as a function of experimental run while Figure 29 is a parity plot showing the experimentally observed reaction rate against predicted reaction rate at 220°C.

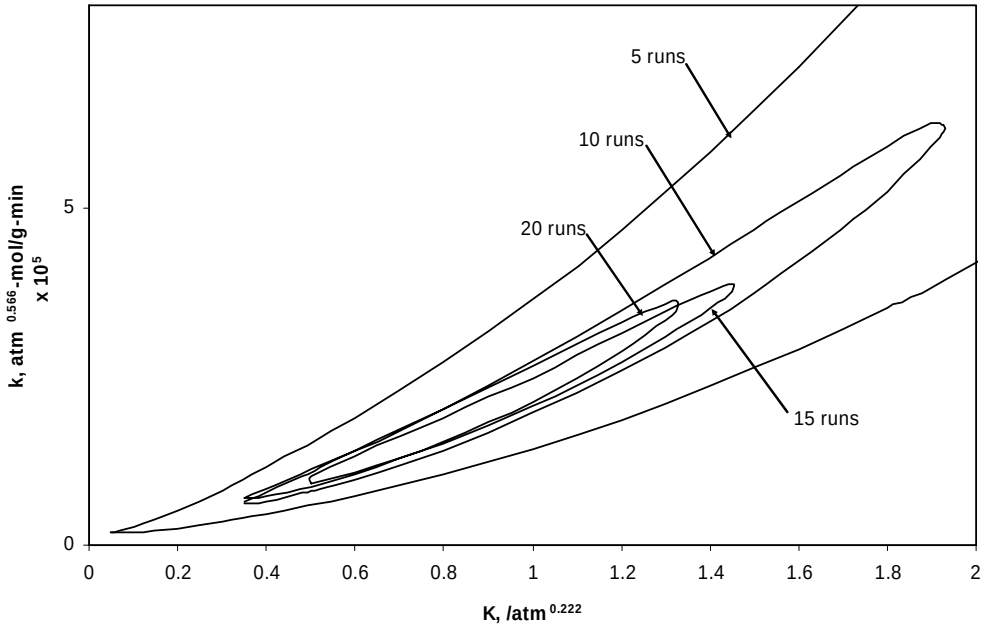

Figure 28. Joint 95% likelihood confidence regions for k, and K at 220°C at different run lengths

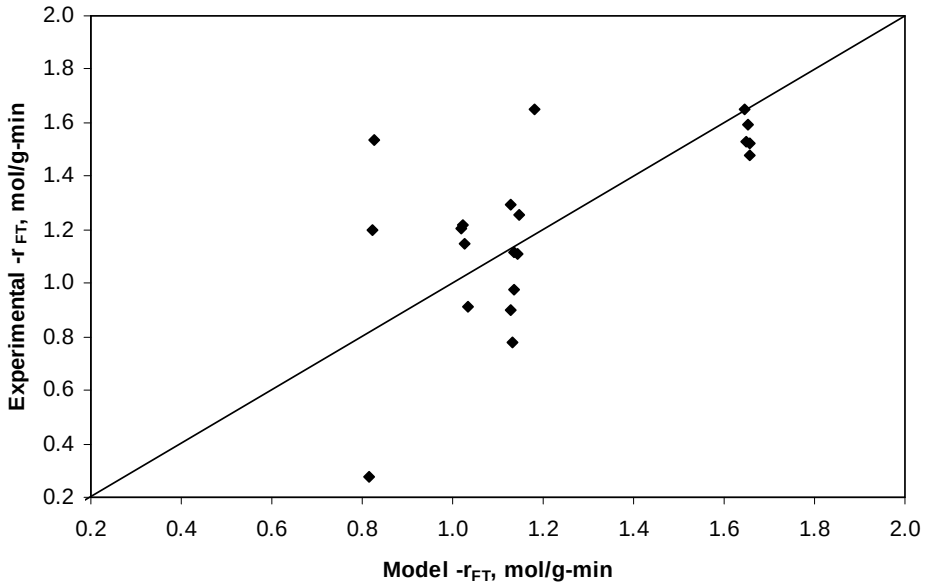

Figure 29. Experimental rates versus model predicted rates for sequentially designed experiments at 220°C.

Similar results were obtained at 239°C. Also, Table 9 shows the regressed values of the activation energy, heat of adsorption and pre-exponential factors.

Table 9. Regressed values of pre-exponential factors, activation energy and heat of adsorption.

	A_1 ($atm^{1.5}$-mol/g-min)	E (kJ/mol)	A_2 (atm x 10^3)	ΔH (kJ/mol)
Parameter Estimate	1205	77.0	4.61	–18.4
Lower 95% Confidence Level	1137	76.8	4.36	–18.6
Upper 95% Confidence Level	1272	77.3	4.89	–18.2

Collection of statistically reliable raw data for the validation of microkinetic model is very essential. Such experimental data should be void of mass transfer effects; also, the parameter space should adequately cover conditions that reflect probable industrial operating conditions.

We chose to use equation 1A to obtain optimized experimental data not just because it was derived by a mechanism that makes sense; but also it predicted rate of hydrocarbon production (C_{2+}) better than other analogs that we tried out.

Each experimental condition was preformed in replicates, to gain more statistical information. This is indicated in the parity plot shown in Figure 29. In this figure, the observed high variance in observed rate values at each replicate point is probably due to our inability to effectively control the reactor temperature due to its large thermo-mass. Nevertheless, it is obvious that the 45 degrees parity line passes through the means at each experimental point.

Perhaps, we could have stopped the collection of data after 15-runs as the value of both the optimality criteria and the estimated constants have very well approached asymptotic values. Moreover, the collection of extra data points improved the statistics only a little.

Results and Discussion based on First Principles Calculations

In the first year of the project we had completed a systematic analysis of the thermodynamics and kinetics of Fischer Tropsch Synthesis (FTS) on a Fe(110) surface. This involved using state-of-the-art First-Principles DFT planewaves-based methods to calculate binding energies (BEs), minimum energy paths, and reaction barriers for key elementary steps in FTS. Subsequently we had started calculations to evaluate the modifying effect of subsurface carbon on the Potential Energy Surface (PES) determined on pure Fe(110). Our calculations indicated that putting a C atom into the first subsurface is relatively facile, especially in the presence of surface oxygen.

Furthermore, findings which indicated that the formation of Fe-carbides was almost a spontaneous process motivated us to investigate the stabilization of various other reactive surface intermediates (coverage of ¼ ML) on the Fe(110) surface in the presence of subsurface carbon. A summary of the calculations we completed during this past year is given in Table 10, and show that this stabilization is indeed observed for all the 19 major intermediates considered. Moreover the magnitude of this stabilization spans a range of values up to a maximum of -0.48 eV for the ethylene (C_2H_4) species. Figure 30 presents these data in a graphical form.

Table 10. Relative strength of binding of adsorbates on *Fe(110)* and *Fe(110) surface modified by subsurface C*, $Fe_C(110)$, at 1/4 ML coverage. All Energies are in eV; a negative sign signifies stabilization of the adsorbates in the presence of subsurface C.

Species	Stabilization due to subsurface C (eV)
H	-0.15
C	-0.09
O	-0.30
CO	-0.16
CO_2	-0.15
CH	-0.24
CH_2	-0.23
CH_3	-0.24
CH_4	-0.04
C_2H_4	-0.48
CCH_3	-0.18
CH_2CH	-0.28
C_2H_6	0
OH	-0.07
H_2O	-0.30
CCH	-0.19
CCH_2	-0.24
$CHCH_3$	-0.20
C_2H_5	-0.25

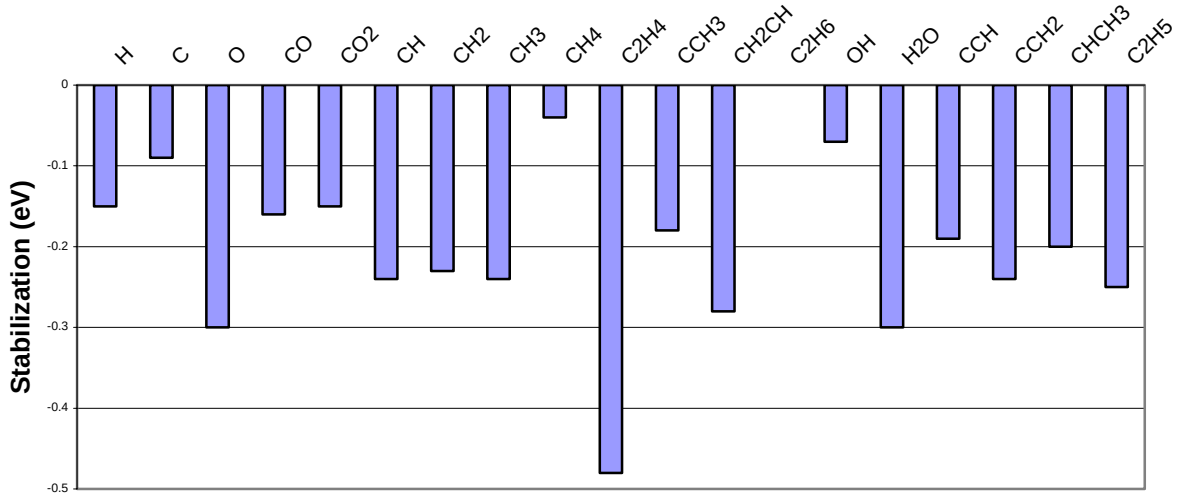

Figure 30. Subsurface C induced stabilization of Fe(110) surface species (1/4 ML coverage)

The next task was to investigate the effect of Pt promotion of FTS on Fe(110). A number of candidate systems were considered but our calculations identified a Fe(110) slab with a Pt adatom as the most promising system in terms of stability. For reference, Figure 31 shows all the three systems studied so far; the Fe(110) system with the Pt adatom is hereafter referred to as Fe^{Pt} , whereas the Fe(110) system with subsurface C in it is called Fe_C.

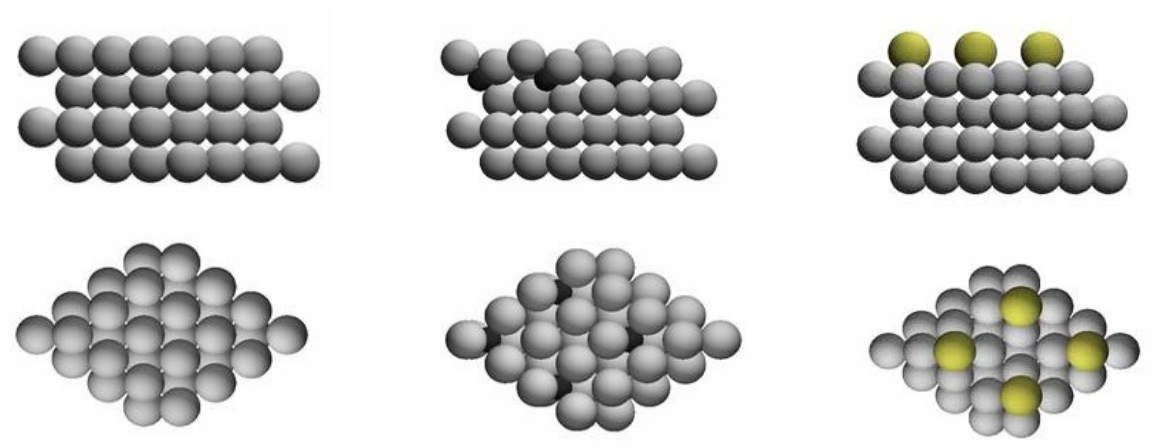

Figure 31. Model Systems for First Principles Calculations of the Potential Energy Surface (PES) for FTS. Top panel gives cross-section views; bottom panel gives top-views of the corresponding slabs.

The Fe^{Pt} system shows behavior in marked contrast to the Fe_C system: Most species are substantially destabilized in the presence of Pt adatoms (Table 11), as opposed to the subsurface C which had a stabilizing effect. At the same time, the behavior presents more species specific variation with respect to the degree of destabilization due to Pt. Figure 32 shows this in greater detail: the destabilization is shown to reach a maximum of 1.1 eV for CCH_3. Remarkably, some species show very little destabilization (C_2H_4) while a few others are actually stabilized (CH_4, C_2H_6, H_2O and C_2H_5).

Table 11. Relative strength of binding of adsorbates on Fe(110) and Fe^{Pt} (Fe(110) surface modified by a ¼ ML coverage of Pt adatoms). All Energies are in eV; positive sign signifies destabilization of the adsorbates in the presence of Pt.

Species	Destabilization in the presence of Pt (eV)
H	0.34
C	0.92
O	1.12
CO	0.47
CO_2	0.38
CH	1.03
CH_2	0.82
CH_3	0.18
CH_4	-0.06
C_2H_4	0.02
CCH_3	1.11
CH_2CH	0.26
C_2H_6	-0.01
OH	1.03
H_2O	-0.14
CCH	0.19
CCH_2	0.11
$CHCH_3$	1.08
C_2H_5	-0.13

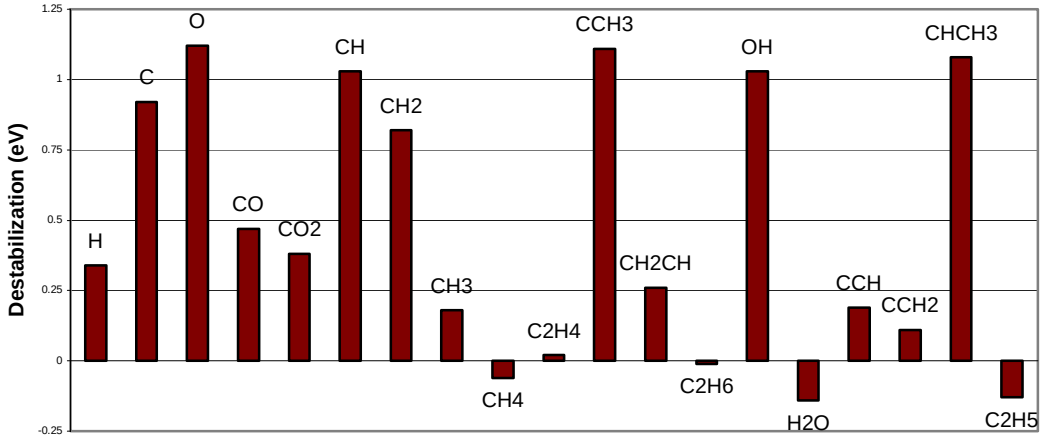

Figure 32. Pt-induced destabilization (positive y-axis) of surface species (Fe(110) – 1/4 ML coverage)

Figure 33 shows the PES for the early steps of FTS (CO dissociation, followed by C hydrogenation up to CH_4 formation) on the three model surfaces studied so far, i.e. Fe(110), Fe_C and Fe^{Pt} . In addition, Figure 33 includes the corresponding PES on a Co(0001) surface we had studied earlier for reference. The above mentioned destabilization manifests itself clearly in Figure 33 and causes the PES for Fe^{Pt} to come closer to the Co(0001) surface. We expect this effect to persist in the later steps of our model (eg. C-C bond formation and the hydrogenation of the C_2 species)

The other major goal achieved during the course of this past year was the calculation of the kinetics of ca. 30 elementary reaction steps on the Fe_C and the Fe^Pt model surfaces. These reactions can be classified into the following major groups:

- CO dissociation CO→C + O
- Stepwise CH_4 formation by successive H additions i.e. C→CH→CH_2→CH_3→CH_4
- C_2 formations involving C-C coupling e.g. C+CH→ CCH, CH+CH→HCCH, C+CH_2→CCH_2, CH_3+CH_3→C_2H_6 (a total of 9 such reactions)
- Hydrogenation of C_2 species e.g. CCH+ H→ HCCH, HCCH + H → CH_2CH, CCH+H→CCH_2,CH_3CH_2+H→C_2H_6 (a total of 9 such reactions)
- Isomerization CH_2CH → CCH_3
- Water formation O + H → OH, OH + H → H_2O, OH + OH → H_2O + O

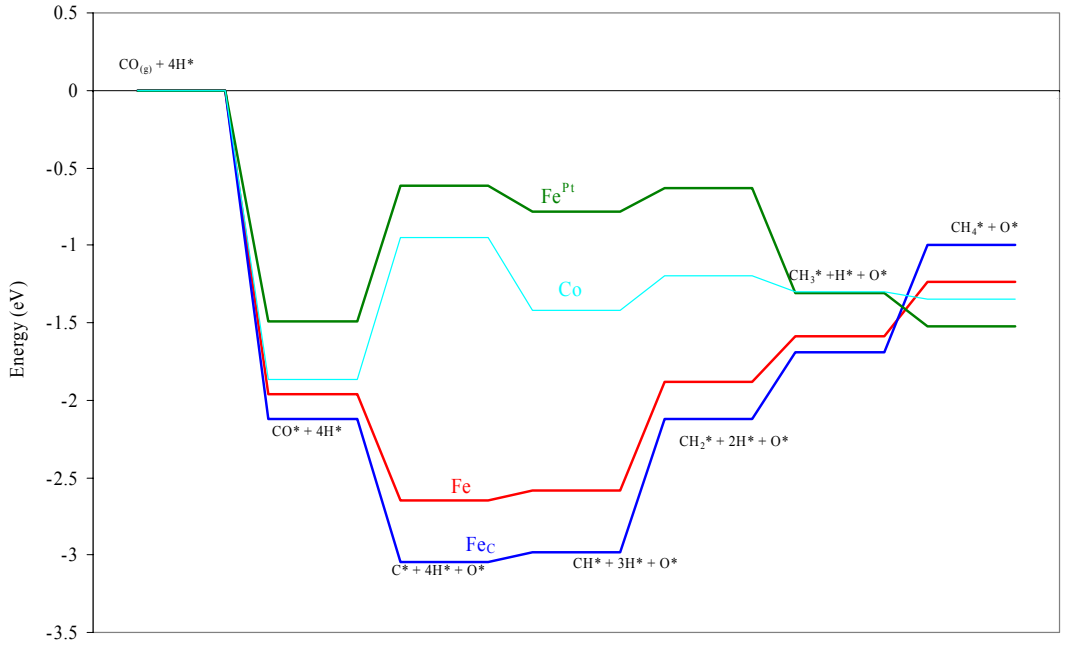

Figure 33. Potential Energy Surface (thermochemistry only) for the early steps of FTS on Fe(110), Fe^{Pt}, Fe_C, and Co(0001).

Overall this yields a complex reaction network, which is represented in Figures 35 for both the Fe_C and Fe^{Pt} systems. For each step shown in that figure we have calculated a kinetic barrier, its corresponding entropy and enthalpy change. It is obvious that, in general, there are multiple possible pathways for the production of most C_2 intermediates and that a final judgment as to the importance of specific pathways can only be made by construction of a detailed microkinetic model. The construction of such a model remains one of our goals for the upcoming year. A simplified view of the more complex PES can be constructed by restricting ourselves to the initial FTS steps, up to CH_4 formation. The modifying effect of the Pt adatom on the pure Fe(110) PES is clearly seen in Figure 34, which includes both thermochemistry and kinetics (TS) data for the respective elementary steps.

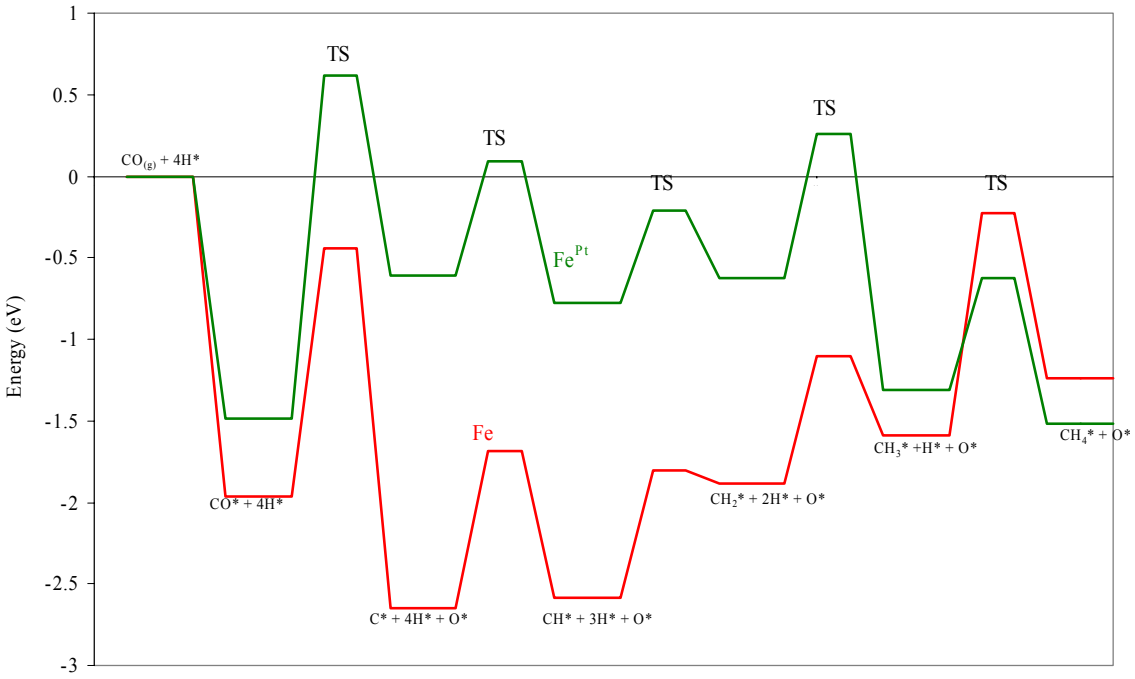

Figure 34. A comparison of the Potential Energy Surface (thermochemistry and kinetics) for the early FTS steps on Fe(110) and Fe^{Pt}.

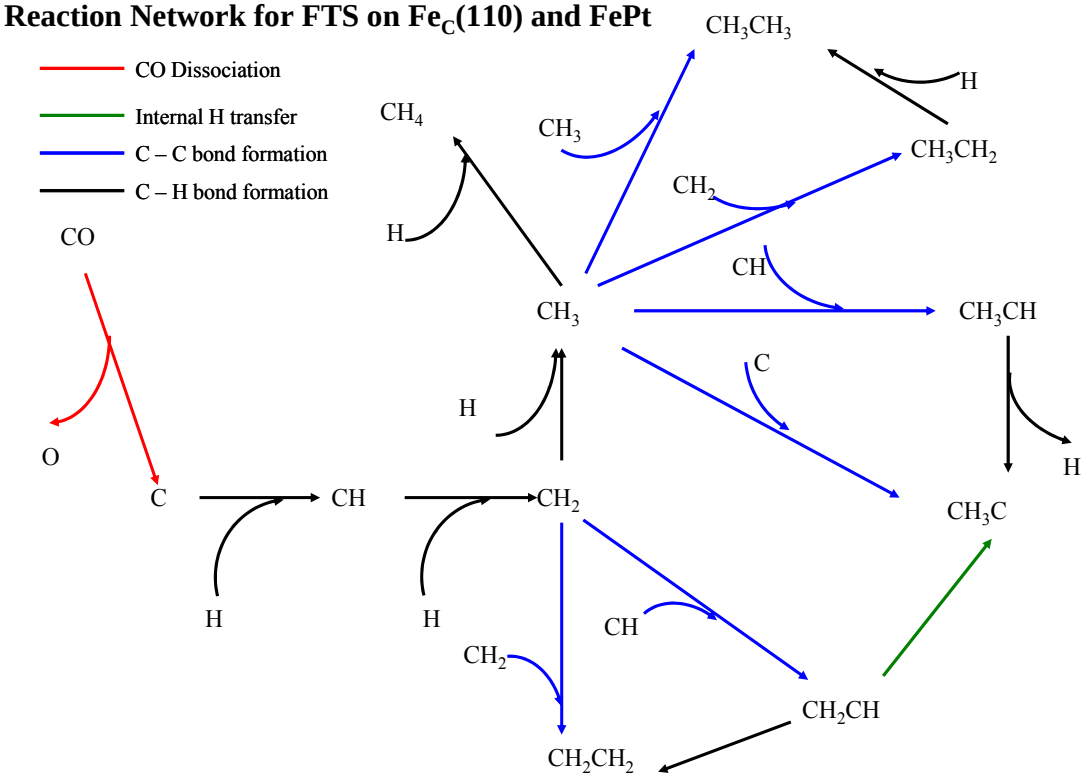

Figure 35. Reaction Network for FTS on Fe_C, an Fe(110) surface with ¼ ML subsurface Carbon, and on Fe^{Pt}, an Fe(110) surface with ¼ ML of a Pt adatoms on it.

In addition, our work in the second year of the project also involved the calculation of vibrational frequencies of stable reaction intermediates and transition state structures, which allows the subsequent calculation of pre-exponential factors for the various elementary steps involved in the reaction mechanism.

As we approach the end of our planned calculations for the Fe^{Pt} model surface, our major target for the next year is to study the effects of steps, or other defects on suitable facets of the single crystal Fe lattice. This, and time permitting, followed by a study of K promotion of FTS would provide us with an enhanced understanding of the early FTS steps (up to C_2 species formation) on Fe, clean and modified surfaces.

Conclusions and Plans

A. Conclusions

1. CO adsorbs molecularly and dissociatively at relatively low temperatures (25-150°C) on polycrystalline iron. K increases the amount of CO adsorbed and its binding energy. Since CO adsorbs dissociatively on polycrystalline Fe at RT, CO dissociation is probably facile under reaction conditions at 250°C, thus, it would not be a rate-determining step under reaction conditions.

2. After FT reaction at 200°C for only 5 minutes, the Fe surface of 99FeA series samples contains many monolayer equivalents of carbidic, amorphous, and graphitic carbon species. Amounts deposited are roughly 10: 2: 1 for Fe/K: Fe/Pt: Fe. Thus, Pt and K facilitate C removal during reaction. Fraction of active carbons on the surface decreases in the order Fe-K, Fe-Pt, Fe. Thus, K and Pt promoters maintain a higher fraction of active carbons on the surface.

3. After FT reaction and during isothermal TPH at 200°C, only 0.15 ML is removed after 2 h from unsupported Fe; rates of α-C removal decrease in the order Fe/K > Fe/Pt > Fe.

4. The alumina support affects CO adsorption mechanism and its binding strength on Fe; for example, the desorption peak temperature of dissociatively-adsorbed CO of 280ºC for a 20Fe/alumina (nonaqueous preparation) is significantly lower than for the unsupported 99Fe catalyst. Moreover, the absence of a high temperature peak (e.g. around 250-400ºC) indicates that CO dissociation does not occur on the 20FeLaA and 20FePtLaA catalysts after CO adsorption at room temperature. Nevertheless, dissociative adsorption of CO is observed on the K-promoted Fe/LaOAl2O3 catalyst, probably because the K promoter enhances CO dissociation. This observation is consistent with observations from previous literature that surface K increases the Fe-C bond strength, thus enhancing CO dissociation.

5. 10% Fe/alumina prepared by aqueous impregnation is significantly more active in FTS than 10 and 20% Fe/alumina catalysts prepared by nonaqueous evaporative deposition. The higher activity of the catalyst prepared by aqueous impregnation is consistent with its (a) larger content of active, atomic, surface carbon and (b) larger Fe crystallites. In the catalyst prepared by nonaqueous means, a significant fraction of Fe crystallites are smaller than 5 nm; crystallites of Fe smaller than 5 nm have been shown to have low activity for FTS.

6. FTS rate data, obtained on alumina-supported iron catalyst in a CSTR reactor at 220-260ºC and 20 atm according to a rigorous statistical sequential design, were fitted to

various rate expressions based on a widely accepted mechanistic sequence of elementary steps. The sequential design procedure resulted in the precise parameter estimates in a minimal number of experiments. Rates of CO conversion s are correlated well by a Langmuir-Hinshelwood expression, derived assuming carbon hydrogenation to CH and OH recombination to water to be rate-determining steps.

7. Density Functional Theory (DFT) Calculations indicated that the Reaction Network for FTS is relatively complex on both systems i.e. (1) Fe(110) with subsurface carbon and (2) Fe(110) with Pt adatoms. These networks were characterized in full detail by evaluating the thermodynamics and kinetics for each elementary step. The dominant trend observed was that subsurface C tends to stabilize all reactive surface intermediates, whereas Pt adatoms tends to destabilize most of them. A detailed microkinetic model utilizing these first-principles parameters should be valuable in deriving rate-limiting steps, reaction-orders, etc, under a wide range of experimental conditions.

B. Plans (coming year)

1. Continue literature search and preparation of review
   a. Search surface scientific literature of iron single crystals.
   b. Update the review of mechanism and kinetics of FTS on iron catalysts and submit for publication.
2. Experimental kinetic and mechanistic studies
   a. Extend kinetic study of FTS to unpromoted 20% Fe/Al_2O_3/monolith and catalyst promoted with K.
   b. Obtain quantitative kinetic parameters for CO dissociation and carbon hydrogenation on unsupported and supported, promoted and unpromoted Fe catalysts.
   c. Conduct isotopic (SSITKA) study of carbon-containing intermediates on unsupported and supported iron catalysts.
   d. Develop a microkinetic model for FTS on Fe.
3. DFT Studies of Elementary Steps
   a. Study the effects of steps, or other defect sites on suitable facets of the single crystal Fe lattice.
   b. Time-permitting, conduct a study of K promotion on Fe-catalyzed FTS.

C. Schedule of Tasks

Table 12. Schedule of Tasks

Task	0-6 mo	7-12 mo	13-18 mo	19-24 mo	25-30 mo	31-36 mo
Task 1. Find kinetic parameters and incorporate in model						
Task 2. Measure kinetic parameters for key elementary steps						
a. Rebuild TPD system and prepare catalysts						
b. TPD, TPSR measurements						
c. Isotopic study						
Task 3. DFT Studies of Elementary Steps on Selected surface models						
Task 4. Collection of rate and selectivity data						
a. Rebuild Berty reactor system						
b. Measure rates and selectivities						
Task 5. Collaborate, write proposals						
Reports	▲	▲	▲	▲	▲	▲
Contractor Meeting		■		■		■

References

1. G. P. Van der Laan, A. A. C. M. Beenackers "Kinetics and selectivity of the Fischer-Tropsch synthesis: A literature review" Catal. Rev. –Sci. Eng. 41 (1999) 255-318.
2. C.H. Bartholomew and R. J. Farrauto, "Fundamental of Industrial Catalytic Processes".
3. K. Yoshida, Japanese Journal of Applied Physics, 20 (1981) 823.
4. K. Ueda, M. Enatsu, Surface Science, 159 (1985) L421.
5. U. Seip, M. C. Tsai, K. Christmann, J. Kuppers, and G. Ertl, Surface Science, 139 (1984) 29.
6. C. E. Bartosch, L. J. Shitman, and W. Ho, J. Chem. Phys. 85 (1986) 1052.
7. K. Ueda, and T. Mega, Japanese Journal of Applied Physics 27 (1988) 2227.
8. D. Bianchi, and J. L. Gass, J. Catal. 123 (1990) 298.
9. Eliason, S. A.; Bartholomew, C. H. In Catalyst Deactivation 1997.
10. M. Claeys, "Effect of Metal Crystallite Size in Supported Iron Based Fischer-Tropsch Catalysts", 19th North American Catalysis Society Meeting, May 22-27, 2005, Philadelphia, Pennsylvania USA.